Hyperspectral and multispectral satellite data analysis of nitrogen in grazed and ungrazed tundra in Långfjället, Sweden

Emma Dahlstedt

Degree of Master of Science (120 credits)
with a major in Earth Sciences
60 hec

Department of Earth Sciences
University of Gothenburg
2023 B1263

Faculty of Science

UNIVERSITY OF GOTHENBURG

UNIVERSITY OF GOTHENBURG
Department of Earth Sciences
Geovetarcentrum/Earth Science Centre

Hyperspectral and multispectral satellite data analysis of nitrogen in grazed and ungrazed tundra in Långfjället, Sweden

Emma Dahlstedt

ISSN 1400-3821

B1263
Master of Science (120 credits) thesis
Göteborg 2023

Mailing address
Geovetarcentrum
S 405 30 Göteborg

Address
Geovetarcentrum
Guldhedsgatan 5A

Telephone
031-786 19 56

Geovetarcentrum
Göteborg University
S-405 30 Göteborg
SWEDEN

Abstract

Reindeer are a keystone species in the circumpolar north, where they hold great cultural and ecological importance. Continued climate change threatens the long-term sustainability of reindeer husbandry. Reindeer can affect the tundra landscape, influencing the soil nutrient cycling, including the soil nitrogen availability. Hyperspectral remote sensing of biochemical traits is a relatively new but promising field of study. This thesis aims to investigate if hyperspectral and multispectral satellite data could be used to differentiate between grazed and ungrazed tundra landscape, as well as to determine which hyperspectral wavelength bands are best suited to estimate nitrogen content over a tundra reindeer grazing site. A hyperspectral satellite, PRIMSA, and a multispectral satellite, Sentinel-2, were used over a heath shrub study site in Sweden. A visual comparison of the spectral curves from PRISMA and Sentinel-2 were used to differentiate between grazed and ungrazed tundra landscape. A variety of remote sensing analysis methods, i.e., PCA, RF regression, RF classification, MLR, and an unsupervised classification, as well as a standard C/N ratio analysis of 24 plant samples were used to get a final map over estimated nitrogen content. The result from this study supports using chlorophyll as a proxy for nitrogen content. From the MLR, all PRISMA wavelength bands below 680 nm (band 35) had R2 values >0.7. In particular, this study identified that band 1, at 405 nm, was best suited for determining nitrogen content over a tundra reindeer grazing site. Neither PRIMSA nor Sentinel-2 were definitively found to be better at differentiating between grazed and ungrazed rangeland. Although this project was limited by the small sample size of the reference data, it shows potential possibilities of what could be done with biochemical trait estimation via remote sensing. Contributing to the wider scientific field by giving a suggested method for estimating nitrogen content and by giving a suggestion for which hyperspectral wavelength band is best suited for determining nitrogen content in a tundra landscape.

Keywords: Hyperspectral imaging, Imaging spectroscopy, Nitrogen, Reindeer, Herbivory, Tundra, Grazing

Acknowledgements

I must begin by expressing my deepest gratitude to my supervisor Heather Reese, who helped me at every step of the way, not only academically, but also through your encouraging words. This project would not have been possible without your guidance. Next, I would like to extend my sincere thanks to my co-supervisor Robert Björk for lending me your expertise and knowledge. Aiding in the fieldwork and the laboratory analysis were also PhD student Cole Brachmann and Danica. I would be remiss if I did not also extend my gratitude for their help during these steps of the process. I also want to extend my thanks to my examiner Mats Björkman, as well as a special mention of fellow master student Jonatan Uusitalo for being my thesis opponent.

I would like to mention Roland Barthel who organized seminars for master students every other Thursday, where he from time to time also gave lectures with seasoned advice about all aspects of writing a master thesis. I want to acknowledge the moral support I got from other students in these seminars, but greater still was the mutual support shared between the students in the Master's thesis room 'Ventifakten'.

Lastly, I want to give thanks to my family for their encouragement throughout the project. I especially want to thank my mother for always believing in me, even on those days when I do not believe in myself.

List of Abbreviations

C/N = Carbon to nitrogen ratio

CWM = Community weighted average/mean

ESA = European Space Agency

IRMS = Isotope-ratio mass spectrometry

MLR = Multiple Linear Regression

MNF = Minimum Noise Fraction

NIR = Near-infrared

PCA = Principal Component Analysis

PLSR = Partial Least Squares Regression

PRISMA = PRecursore IperSpettrale della Missione Applicativa

RF = Random Forest

SWIR = Short-wave Infrared

UV = Ultraviolet

VIS = Visible Spectrum

Table of Contents

1. Introduction

The northern most latitudes are experiencing a phenomenon known as Arctic amplification, i.e., the Arctic surface air temperatures are warming twice, up to possibly four times, as fast as the global average (Meredith et al., 2019; Rantanen et al., 2022). Reindeer herders are vulnerable to continued climate change (Furberg et al., 2011), which can adversely affect reindeer husbandry through increased rain-on-snow events and shrubification (Meredith et al., 2019). Reindeer hold fundamental cultural and socioeconomical importance to the indigenous populations in the North (Holand et al., 2022; Vors & Boyce, 2009). Simultaneously, reindeer also hold great importance to the tundra landscape, where reindeer can influence the soil nutrient cycling through food selection, trampling, and excreta (Stark et al., 2023). These mechanisms affecting the nutrient cycling can inhibit or enhance nitrogen availability (Stark et al., 2023), which is important, as regions in the northernmost latitudes have soils where nitrogen is a limiting nutrient (Reich & Oleksyn, 2004).

During winter conditions the diet of reindeer are very dependent on lichens (Inga, 2007; Staaland & Saeboe, 1993; Tunón & Sjaggo, 2012). Lichens are nitrogen poor, so reindeer supplement by foraging on other plants, mostly shrubs (Inga, 2007; Staaland & Saeboe, 1993). Biochemical and biophysical traits in vegetation affects its spectral properties (Cavender-Bares et al., 2020). Nitrogen displays absorption features in the short-wave infrared range (because of nitrogen proteins) and chlorophyll (which can be used as a proxy for nitrogen content) affects the visible spectrum up to the red edge (Kokaly et al., 2009). Previous research into nitrogen trait remote sensing have primarily used methods focused on chlorophyll content, while fewer articles have investigated nitrogen at longer wavelengths (Berger et al., 2020a). Biophysical variable analysis (e.g., chlorophyll) alongside vegetation classification are the two main applications of hyperspectral imaging in the Arctic (Liu et al., 2017a).

A hyperspectral satellite, PRIMSA, and a multispectral satellite, Sentinel-2, were used over a tundra heath site in Sweden to analyse nitrogen in grazed and ungrazed environmental treatments. Hyperspectral remote sensing is defined by a high number of narrow wavelength bands over a continuous spectrum (Eismann, 2012; Kramer, 2003). In contrast, multispectral sensing does not cover a continuous spectrum and uses fewer and broader wavelength bands (Eismann, 2012). Much of the hyperspectral remote sensing of biochemical traits has been carried out over forest and agricultural ecosystems (Van Cleemput et al., 2018). The literature is scarcer for hyperspectral remote sensing of biochemical traits in shrublands and grasslands (Van Cleemput et al., 2018).

1.1 Aim and Objectives

The aim of this project was to investigate if hyperspectral satellite data could be used to differentiate between grazed and ungrazed tundra landscape, as well as estimate nitrogen content of the vegetation over this landscape. The project was motivated by the potential to aid in the long-term sustainability of reindeer husbandry.

To accomplish this aim, I investigated the following objectives: to (1) determine which hyperspectral wavelength bands are best suited for determining nitrogen content from vegetation measured over a tundra reindeer grazing site and (2) to investigate if the PRISMA hyperspectral sensor can more accurately differentiate between grazed and ungrazed tundra vegetation than the Sentinel-2 multispectral sensor.

1.2 Remote sensing

A common definition of remote sensing is as “the field of study associated with extracting information about an object without coming into physical contact with it“ (Schott, 2007, p. 1). This is a broad definition which encompasses more than just Earth observation (Schott, 2007), which is what the term remote sensing refers to in the context of this paper. When electromagnetic radiation is used in remote sensing techniques, sensors can be divided into either passive or active sensors. Passive sensors register naturally reflected electromagnetic radiation to capture the reflectance properties of a target (Eismann, 2012; Kramer, 2003). Active sensors produce their own source of electromagnetic radiation and then measure the reflectance properties from the target (Eismann, 2012; Kramer, 2003).

For Earth observation using passive sensors, the range of interest (400-14000 nm) lies within the optical section of the electromagnetic spectrum (Eismann, 2012). This includes the following subregions of the optical section: visible spectrum (VIS) 400 – 700 nm, near infrared (NIR) 700-1300 nm, shortwave infrared (SWIR) 1300-3000 nm, midwave infrared 3000-6000 nm, and thermal/long wavelength infrared 6000-14000 nm (Kramer, 2003). Passive sensors can utilize the VIS, NIR, and SWIR ranges during daytime to measure reflected sunlight, and the long wavelength infrared region at any time of day or night to measure thermal emissions (Eismann, 2012).

Remote sensing platforms can be divided into ground based, aerial, and spaceborne. For spaceborne Earth observation the first satellite designed for this purpose, Landsat-1, was launched in 1972 (Kramer, 2003). In the 1980s the first airborne hyperspectral imaging spectrometers were flown using airplanes, while hyperspectral satellites began orbiting the Earth towards the end of the 1990s, e.g., the Hyperion satellite was launched in 2000 (Kramer, 2003).

Passive multispectral and hyperspectral instruments are based on the same concept of dividing the measured radiation from an imaged target into various wavelength bands (Kramer, 2003). While multispectral sensing uses fewer and broader wavelength bands, which are discrete and usually discontinuous in character (Eismann, 2012), hyperspectral imaging collects a higher number of narrow wavelength bands (>20 bands up to hundreds of bands) over a continuous spectrum (Eismann, 2012; Kramer, 2003). The spectral bands from a hyperspectral sensor (PRISMA) and a multispectral sensor (Sentinel-2) are displayed in Figure 1.

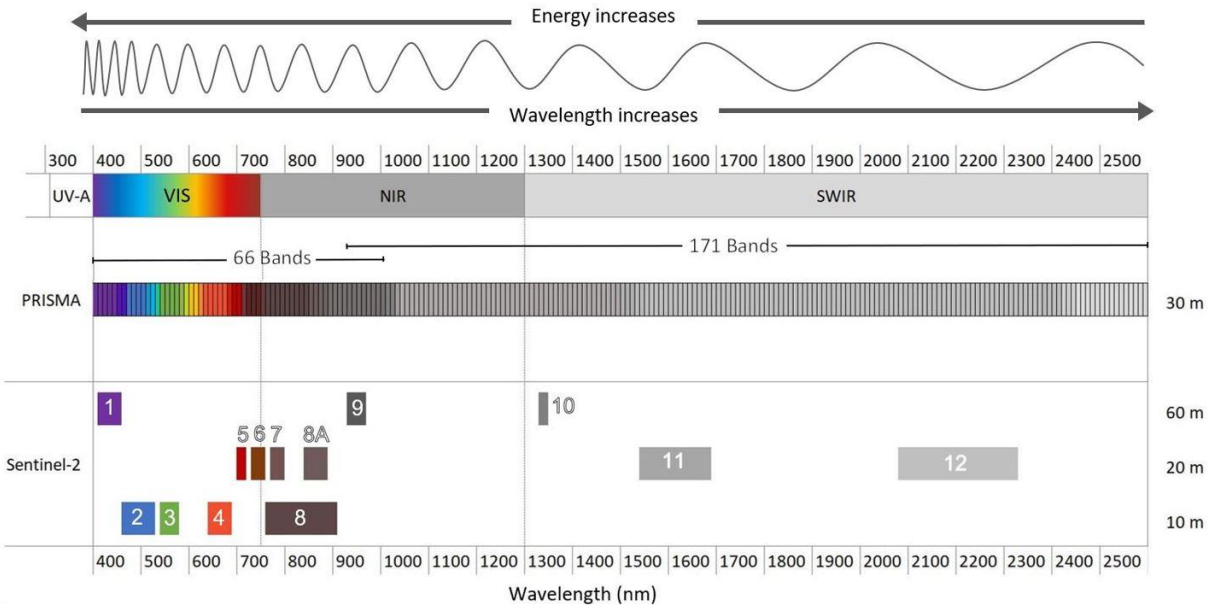

Figure 1. *Illustration of the difference in spectral resolution between a hyperspectral sensor (PRISMA) and a multispectral sensor (Sentinel-2). The image is inspired by Figure 2 in Niroumand-Jadidi et al. (2020). The Sentinel-2 numbers refer to the wavelength bands names. While the number over the continuous PRISMA bands refer to the amount of hyperspectral wavelength bands (Loizzo et al., 2018). The spatial resolution is displayed on the right hand side of the figure. PRISMA also has one panchromatic band of 5 m resolution (Loizzo et al., 2019), which is not shown in the figure.*

1.2.1 Spectral signature curves of vegetation

The reflected radiation in the ultraviolet (UV) and VIS range is shaped by electron processes, which require more energy than vibrational processes that shape absorption features in the NIR and SWIR range (Schott, 2007). Photosynthesis is an electron processes in plants, where the electron transition occurs when VIS sunlight is absorbed by leaf pigments (Eismann, 2012). Vegetation also absorbs infrared radiation which is used for leaf transpiration, and a small percentage of the total energy vegetation absorbs is UV radiation which causes fluorescence (Eismann, 2012) through photosynthesis (Kramer, 2003).

For vegetation, photosynthesis by foliar pigments cause high absorption and low reflectance in the VIS (Eismann, 2012). The main leaf pigment that drives photosynthesis is chlorophyll, while another significant contributing pigment is xanthophylls (Eismann, 2012). Chlorophyll a and b are complex pigments which during the electron transition required for photosynthesis, leave broad absorption features in blue and red wavelengths (Eismann, 2012). This causes a green peak close to 550 nm, as can be seen in a spectral signature curve for vegetation (e.g., Figure 2), and is the reason why we perceive plants as green (Eismann, 2012). At 700 nm the absorbance of photosynthesis pigments ceases and a sharp increase in reflectance can be observed (Figure 2), known as the red edge (Eismann, 2012).

In contrast to the VIS, the NIR and SWIR ranges display higher reflection due to scattering in the internal structure of leaves, and absorption features caused by vibration processes of foliar components (Cavender-Bares et al., 2020; Eismann, 2012). In the NIR spectrum, vegetation displays high reflectance and low absorbance (Figure 2) which is attributable to the influence of water absorbance and leaf structure (Eismann, 2012). Scattering is caused by the internal leaf

structure, i.e., the composition of air spaces and plant cells, and is the foremost reason for the high reflectance in NIR (Eismann, 2012). To specify further, light is scattered within the internal structure of the leaves but low absorbance results in higher reflectance over the NIR region compared to the adjacent VIS and SWIR subregions (Cavender-Bares et al., 2020).

Water absorbance is the main process influencing spectral features in the SWIR range (Eismann, 2012). All wavelengths above 1400 nm are influenced by water absorption (Cavender-Bares et al., 2020). In addition, the SWIR region is also affected by absorbance features from other foliar components, i.e., cellulose, lignin, proteins (such as nitrogen), sugars, starch (such as pectin), and waxes (Cavender-Bares et al., 2020; Eismann, 2012).

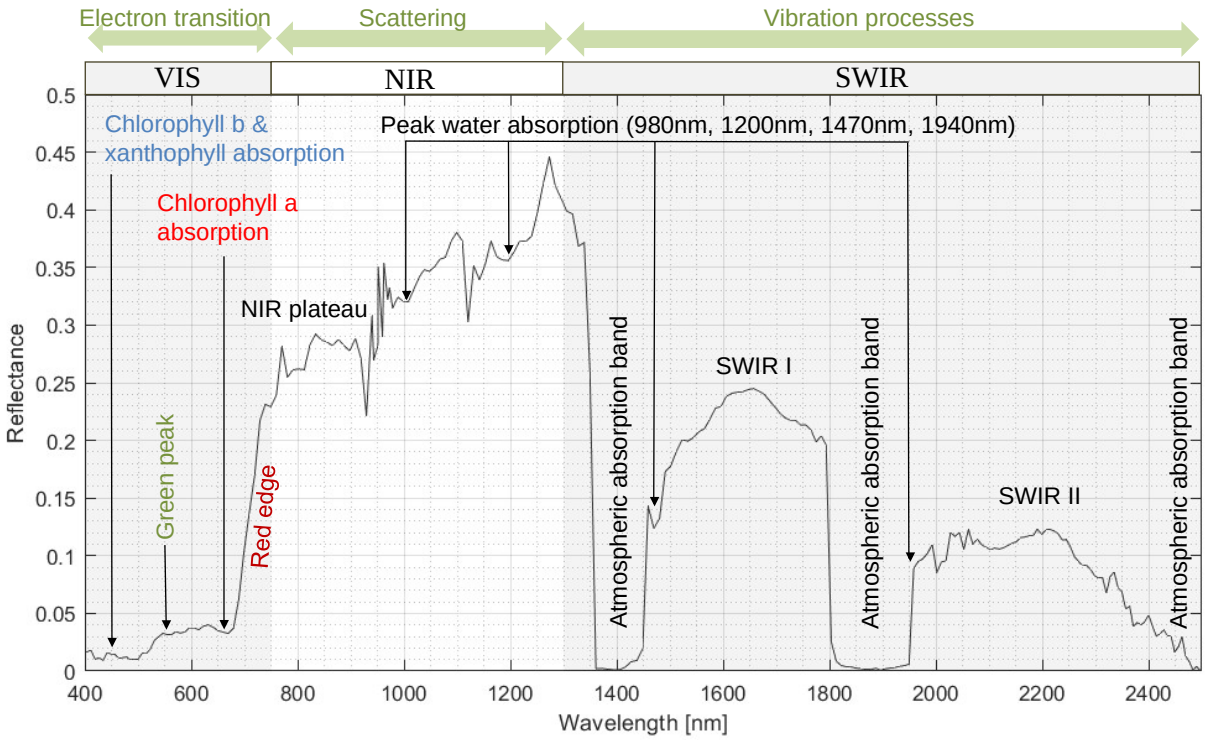

Figure 2. *A spectral signature curve of vegetation. The green divisions at the top of the graph present the main driving processes of that electromagnetic subregion. There are other influences not displayed in the illustration, e.g., that of other foliar constituents besides leaf pigments and water. The black unsmoothed spectral signature curve is taken from PRISMA data over Plot 1 (a reindeer grazing exclosure) in the study area in Långfjället. The figure is based on information from Eismann (2012).*

1.2.2 Remote sensing of nitrogen

Nitrogen in plants forms proteins (e.g., rubisco) and is a component of chlorophyll (Kokaly et al., 2009). Nitrogen displays absorption features in the SWIR range because of nitrogen proteins, while chlorophyll affects the VIS range up to the red edge and can be used as a proxy for nitrogen content (Kokaly et al., 2009). Much of the previous research into nitrogen trait remote sensing has focused on methods using the correlation between nitrogen and chlorophyll content, while fewer articles have investigated nitrogen through the NIR-SWIR range (Berger et al., 2020a). Additionally, much of the hyperspectral remote sensing of biochemical traits literature has been carried out over forest and agricultural ecosystems and there is only a relatively small body of literature covering shrublands and grasslands (Van Cleemput et al., 2018).

Absorption features connected with electron transfer in photosynthesis include a larger peak at 460 nm and a weaker peak at 640 nm for Chlorophyll b, and a weaker peak at 430 nm and a stronger peak at 660 nm for Chlorophyll a (Curran, 1989). The values for chlorophyll absorption features above refer to their central wavelengths. However, observed reflectance tends to be closer to the asymptote of each absorption feature, which is slightly displaced from the central wavelength, e.g., at 685-700 nm for chlorophyll a (Curran, 1989; Mutanga et al., 2003). Absorption features, due to vibrational processes in nitrogen containing proteins, have been found at wavelengths: 1020 nm, 1510-1520 nm, 1730 nm, 1960-1980 nm, 2055-2060 nm, 2130 nm, 2172-2180-2200 nm, 2240 nm, and 2290-2300 nm (Curran, 1989; Fourty et al., 1996; Kokaly, 2001).

1.3 Reindeer

Reindeer (*Rangifer tarandus* L.) are large herbivores that act as a keystone species for its geographical distribution range in the circumpolar north (Holand et al., 2022). In this region, *Rangifer* and muskoxen (*Ovibos moschatus*) constitute the only native ungulates (Holand et al., 2022). While subspecies of *Rangifer* have been classified, there are no other species than *Rangifer tarandus* L. in the *Rangifer* genus (Bernes et al., 2015; Holand et al., 2022). In Eurasia, reindeer refers to both domesticated and undomesticated *Rangifer*, while in North America wild *Rangifer* native to the continent are referred to as caribou whereas reindeer refers to domesticated *Rangifer* originating from Eurasia (Cronin et al., 2003). *Rangifer* carries great significance for both the ecosystem (e.g., through influencing nutrient cycling) and for indigenous populations (i.e., it holds fundamental cultural and socioeconomical importance) in the North (Holand et al., 2022; Vors & Boyce, 2009).

1.3.1 Large herbivores and climate change

A review paper by Soininen et al. (2021) found that most articles investigating the effects of herbivores in the Arctic were from Fennoscandia and the Subarctic, i.e., there are fewer studies conducted over colder and dryer continental Arctic regions. They found that most studies were done on vertebrate herbivores as opposed to invertebrates, and among the vertebrates *Rangifer a*ccounted for the majority of the studies. There is also a tendency to rely on exclosures for studies on herbivores' effect on the Arctic landscape, which excludes other scenarios, e.g., increased grazing or reduced grazing scenarios (Soininen et al., 2021).

The northern most latitudes are experiencing faster rising surface air temperatures than the global average, this phenomenon is known as arctic amplification and is occurring with a magnitude of a minimum of twice the global average (Meredith et al., 2019), and possibly up to four times greater warming according to a recent study (Rantanen et al., 2022). According to a special report by the Intergovernmental Panel on Climate Change, reindeer herding can be affected by climate change through increased rain-on-snow events, which would prevent access to ground vegetation, and shrubification, which would expand cover of poor forage (Meredith et al., 2019). Documented observed adaptations include changing migration patterns, extending forage ranges, and utilizing supplemental feeding during cold months (Meredith et al., 2019).

1.3.2 Reindeer forage and nitrogen

Reindeer are able to forage on most of the plants found within its distribution range (Eriksson et al., 2007) and although they are selective when grazing, they also adapt foraging according to the seasons, following a circannual rhythm for their energy needs (Holand et al., 2022). Sámi reindeer herders divide the year into eight seasons: Spring, spring-summer, summer, fall-summer, fall, fall-winter, winter, and spring-winter (Tunón & Sjaggo, 2012). During winter conditions the diet of reindeer is very dependent on lichens (Inga, 2007; Staaland & Saeboe, 1993; Tunón & Sjaggo, 2012). According to Sámi reindeer herders, among ground lichens, reindeer are partial towards *Cladonia* species and are less inclined to forage *Nephroma arcticum* and *Stereocaulon pascale*, two nitrogen-fixing lichens (Inga, 2007). The availability of lichens on trees are especially important for when ground lichens are covered by a thick ice crust, which inhibits ground grazing (Tunón & Sjaggo, 2012). Lichens provide a lot of energy but are mineral and nitrogen poor, so in the colder months reindeer supplement by foraging on other plants (mostly shrubs), such as *Empetrum* species, *Vaccinium myrtillus*, and *Vaccinium vitis-idaea*, to meet their nutritional requirements (Inga, 2007; Staaland & Saeboe, 1993). While lichens can be consumed by reindeer during warmer months (Inga, 2007), their preferences shifts towards more nutrient rich green vegetation as it emerges (Tunón & Sjaggo, 2012). Reindeer mostly forage on graminoids, forbs, roots, mushrooms, and deciduous leaves during the warmer seasons when the ground is not covered in snow (Tunón & Sjaggo, 2012). Even under snow cover, in late fall, foraging of mushrooms has been observed by reindeer herders (Inga, 2007).

Stark et al. (2023) suggested that future research with the aim to investigate herbivores' effect on the ecosystems should address both the historical land-use of the study site and the present-day processes which are affecting the landscape. How reindeer can affect the tundra landscape, i.e., through food selection, trampling, and excreta, is illustrated in Figure 3 (Stark et al., 2023). These mechanisms affect the nutrient cycling in the soil, however whether the interactions inhibit or enhance nitrogen availability is very context dependent, e.g., on the pasture's grazing history and the current grazing intensity (Stark et al., 2023). Pape and Löffler (2012) submitted that the largest external processes which impact reindeer husbandry are pasture degradation (related to overexploitation), climate change, land-use conflicts, and predators. They also present that an additional influencing factor is the socioeconomical and political conditions, where in Sweden the government has managed pasture distribution and reindeer herd extent.

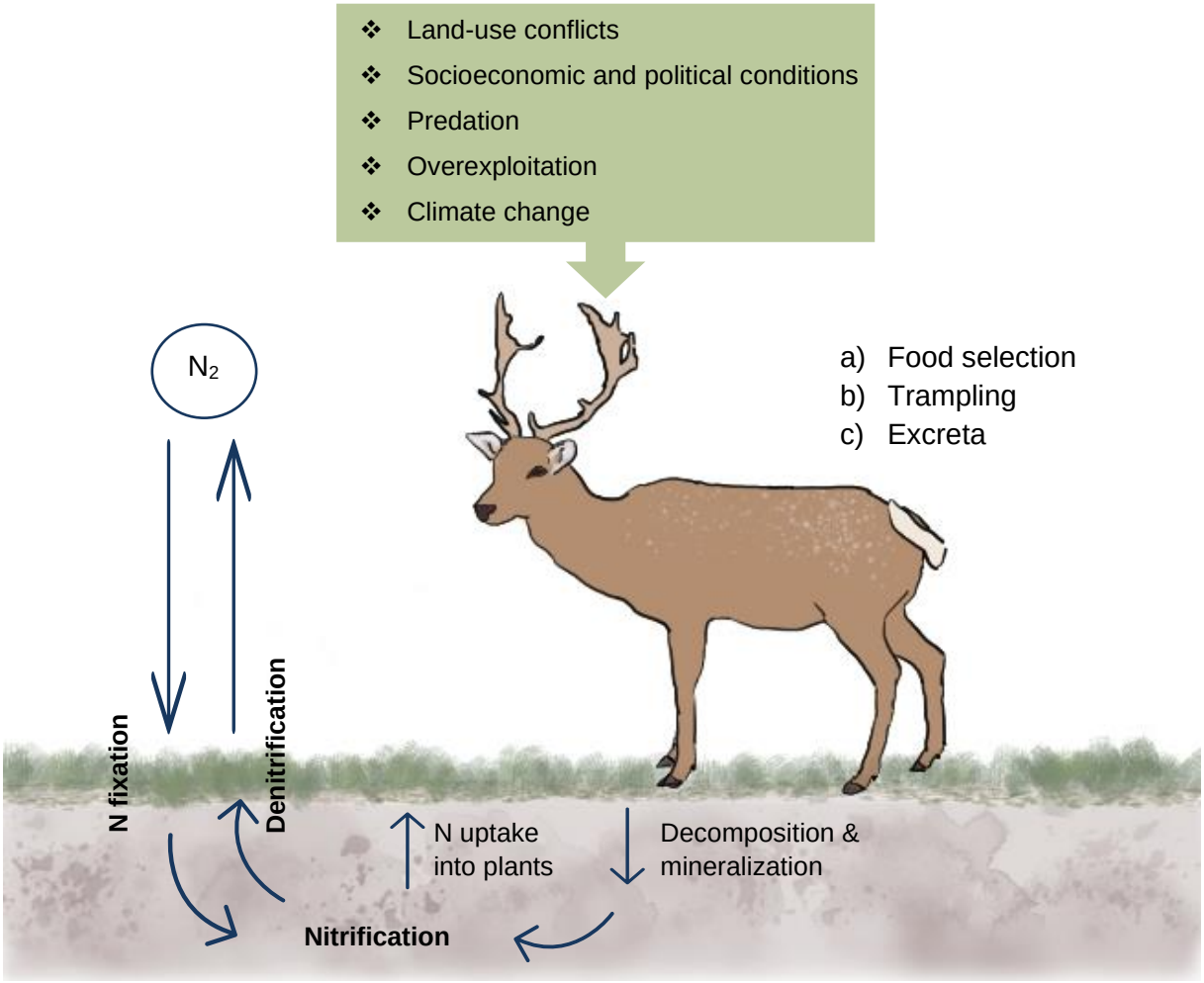

Figure 3. *Overview of some processes which affect reindeer husbandry and how reindeer can impact the tundra ecosystem, with a special focus on the impact on nitrogen cycling. Processes which influence reindeer husbandry, from Pape and Löffler (2012), are shown in the green box at the top of the figure. Reindeer can affect the tundra landscape through primarily three processes: through (a) food selection, (b) trampling, and (c) excreta (Stark et al., 2023). To the left in the figure, a simplified diagram of the nitrogen cycle is illustrated. The bold black text displayed indicates the three main processes in the nitrogen cycle: nitrogen fixation, nitrification, and denitrification (Stein & Klotz, 2016). Shown in the figure is also an arrow indicating the decomposition and the mineralization related to the added nitrogen through reindeer feces and urine (Stark et al., 2023).*

1.3.3 Reindeer in Långfjället

The grazing reindeer herds in Långfjället belongs to "*Idre nya sameby*" (Idre new Sámi village) which was re-established in 1983 and is the southernmost Sámi village in Sweden (Lantbruksnämnden i Jämtlands län, 1990). In the years shortly following its revival, Idre new Sámi village received a cap of maximum 2 700 reindeer in its winter herd (Lantbruksnämnden i Jämtlands län, 1990). The reconstruction of the Idre new Sámi village, nearly 40 years ago, implies that an older Idre Sámi village was once present. Idre and other nearby Sámi villages are believed to have an equivalent long tradition in reindeer husbandry (Samefolkets Egen Tidning, 1926). However, reindeer husbandry was stopped in Idre Sámi village in 1923 when the Reindeer grazing convention between Sweden and Norway was enacted, because Swedish

reindeer would often cross over the border into Norway (Samefolkets Egen Tidning, 1925). Whereas Sámi in Idre at the time argued for resurrecting a fence to resolve the issue and to provide a mutually beneficial solution (Samefolkets Egen Tidning, 1925). Already in the early 20th century reindeer grazing sites in the north were deteriorating, and so contemporary reindeer herders viewed it as a loss to close reindeer herding in an area like the one in Idre, which was very lichen rich, rarely experienced ice crust issues (a big issue further north), and the land had the potential to sustain furthermore reindeer (Samefolkets Egen Tidning, 1926). Idre Sámi village is a "*Fjällsameby*" (Mountain Sámi village), which is a classification referring to Sámi reindeer herders who, in contrast to forest Sámi, typically are more dependent on reindeer husbandry for their livelihood and are also characterized by greater distance travelled for seasonal migration from spring-summer-autumn grazing in the mountains above the tree line, to winter grazing in coniferous forests (Eriksson et al., 2007).

In the past, the vegetation in Långfjället has undergone vegetation transitions. Sometime between early-1980s to mid-1990s a vegetation shift from grass heath to dry heath appears to have occurred at the study site. Rafstedt (1982, as cited in Vowles et al., 2017b) describes a graminoid dominated heath site, while a little over a decade later, in 1995, low shrubs had started to exceed graminoids (Eriksson et al., 2007). Prior to this transition, the vegetation in Långfjället underwent a shift from a mountain crowberry wind heath to grass heath, and one of the objectives Eriksson et al. (2007) intended to investigate was if it would retransition from a graminoid-dominated site back into a shrub-dominated state if the high reindeer grazing pressure was removed. According to inventories taken in 2011, when Vowles et al. (2017b) revisited the site, the shrubification trend continued. Their results showed an increase in shrubs in both exclosures and ambient plots established in 1995. Thus this continued retransition into a shrub-dominated state does not appear to be driven by reindeer grazing pressure (Vowles et al., 2017b). As suggested by Vowles et al. (2017b) the change in vegetation composition could possibly be attributed to environmental drivers, such as observed increase in air temperature and longer growing seasons.

2. Method and Materials

2.1 Study area

The fieldwork was carried out at an established shrub heath study site, located near Lake Grövelsjön in Långfjället, Sweden [62º06′52″N, 12º16′14″E], Figure 4. Located at the southern part of the Scandinavian Mountains in Sweden within the county of Kopparberg in the province of Dalarna. The climate in this region is classified as Dfc, Subarctic Climate, according to the Köppen-Geiger Climate Classification (Beck et al., 2018). The mean annual temperature and precipitation over Idre, where the nearest active weather observation stations to Långfjället are located, was +1.5 ºC and 615 mm respectively, calculated in conjuncture with the climograph, Figure 5 (Swedish Meteorological and Hydrological Institute [SMHI], n.d.). The study area is located on a slope facing eastward and with elevations ranging from 840 to 860 m a.s.l., extrapolated from elevation data from Lantmäteriet (n.d.). The study area in Långfjället has six plots, Figure 6, which were established as part of a World Wildlife Fund (WWF) project in 1995 (Eriksson et al., 2007).

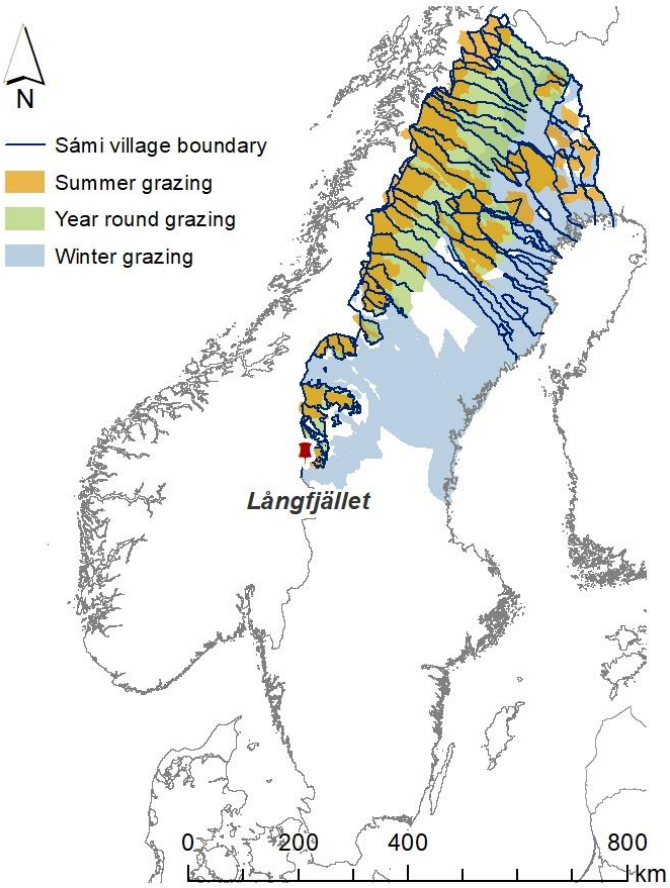

Figure 4. *The map shows the location of Långfjället study area. Seasonal grazing ranges and administrative boundaries of the Sámi villages are also drawn on the map. These shapefiles were collected from (Sametinget, 2016), while county administrative borders are from DIVA-GIS (http://www.diva-gis.org/gdata).*

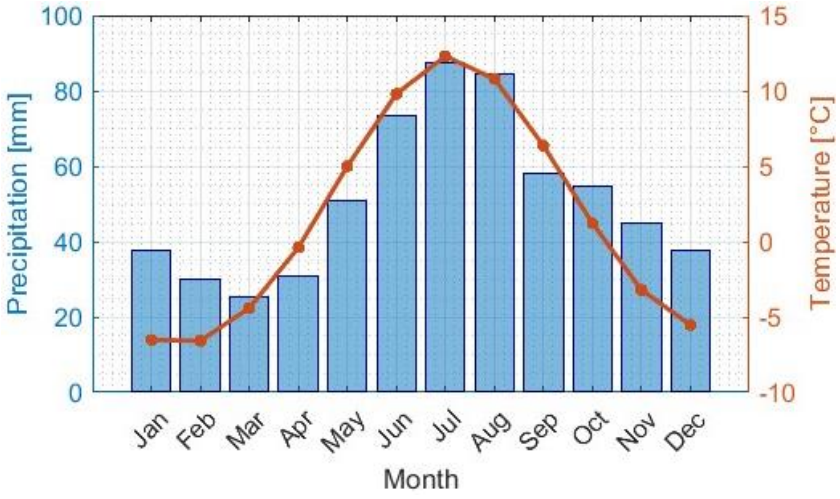

Figure 5. *A climograph (1985-2022) shows averaged monthly air temperature and precipitation from SMHI stations Idre Fjäll A (37,2 km from the study site) and Idre D (39,6 km from the study site) respectively (SMHI, n.d.).*

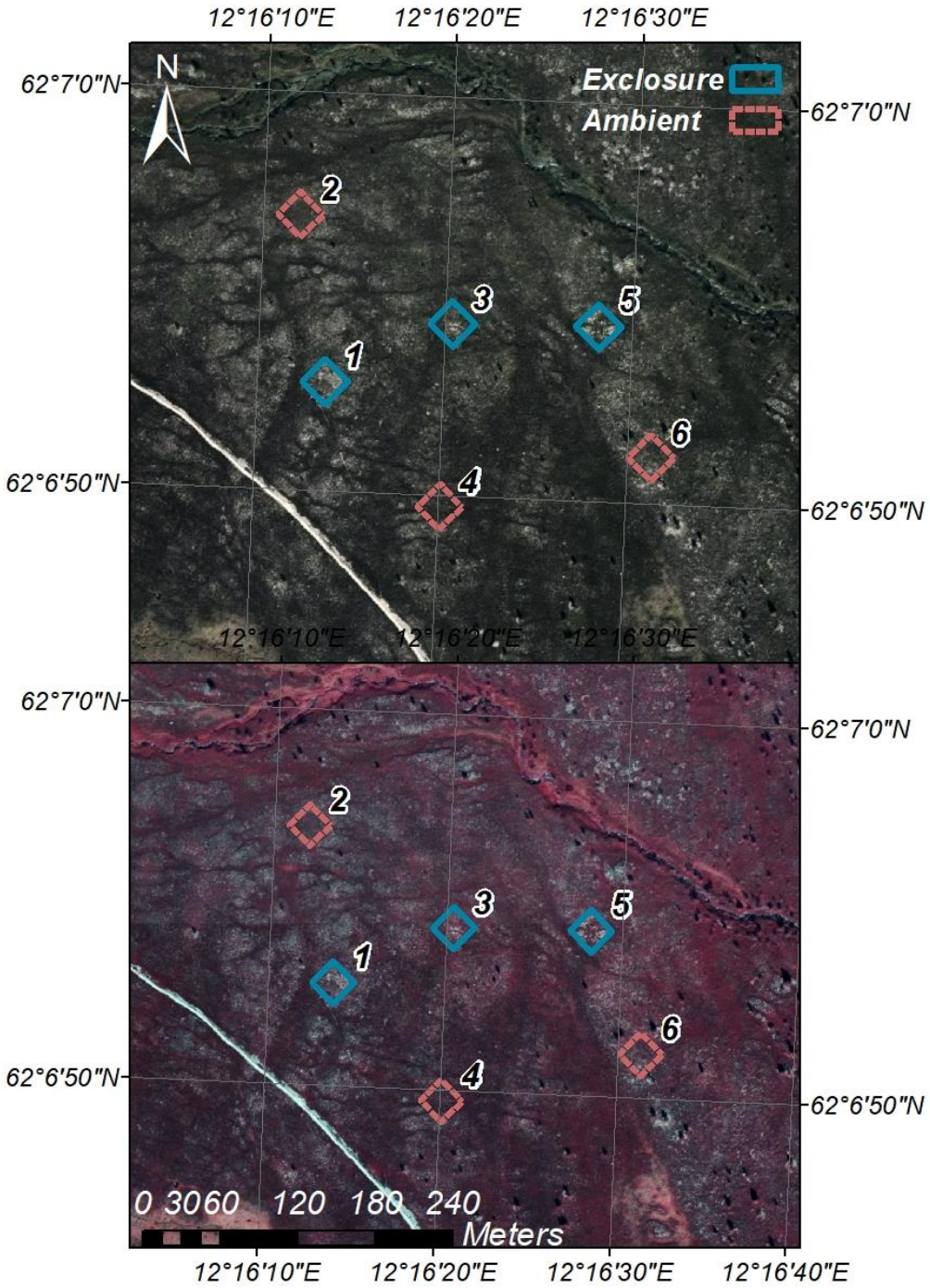

Figure 6. *The study area, Långfjället, and the six established plots are displayed over a 'True Color' (top figure) background and a 'False Color' (bottom figure) image. Background orthophotos are from (Lantmäteriet, n.d.).*

The vegetation at Långfjället study site is a dry heath (Eriksson et al., 2007), see Figure 7. The dry heath in Långfjället's field layer is dominated by evergreen and deciduous shrubs. Evergreen shrubs like *Empetrum hermaphroditum* (Crowberries), *Calluna vulgaris* (Common heathers) and *Vaccinium vitis-idaea* (Lingonberries), and deciduous shrubs like *Betula nana* (Dwarf birch) and *Vaccinium myrtillus* (European blueberry) are common, along with graminoids (grass-like plants). Inside the study plots, *Rubus chamaemorus* (Cloudberry) and *Arctous alpina* (Alpine bearberry) were also discovered. The bottom layer is dominated by

Cladonia rangiferina (Reindeer lichen) and byrophytas, additionally *Cetraria islandica* (True Iceland lichen) was found within the plots (ref. Field observations). The vegetation at Långfjället is limited by the underlying nutrient poor Dala-granite bedrock (Eriksson et al., 2007). The Dala-granite is acidic and highly weathered, resting on top of the bedrock is a layer of gravelly till, which connects to an overlying podzol soil profile (Eriksson et al., 2007).

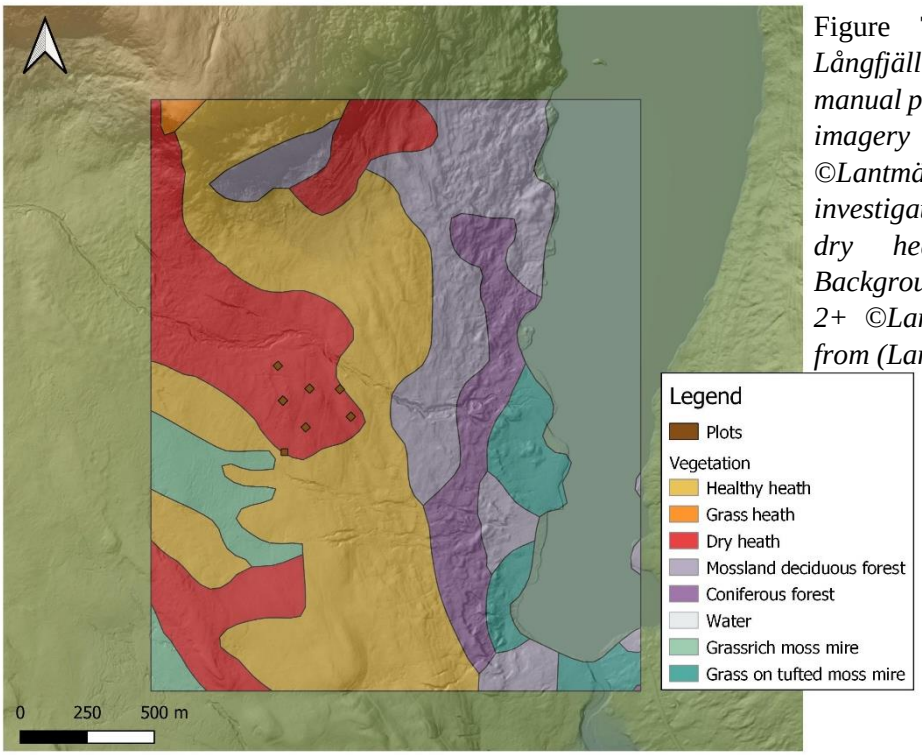

Figure 7. *Vegetation cover of Långfjället, Sweden, based on manual photointerpretation of aerial imagery in the alpine region ©Lantmäteriet. The plots that were investigated in field are located on a dry heath tundra landscape. Background: Elevation data, Grid 2+ ©Lantmäteriet. Data retrieved from (Lantmäteriet, n.d.).*

The fieldwork was carried out during early August 2022, at a heath shrub study site in Långfjället. The field study site at Långfjället has six established plots, which at the time of the field campaign had been in use for 27 years. Each of the plots in the site are 25 x 25 m in size. Out of the six plots, three are fenced exclosures designed to keep large herbivores out. The remaining three plots are paired control plots, operating under ambient open conditions. To identify the location of the ambient plots, all corners had a 90º angled 'V' indent. Further information on the study site can be found in Eriksson et al. (2007). The fieldwork and all the analysis included in the method is illustrated in a workflow diagram (Figure 8).

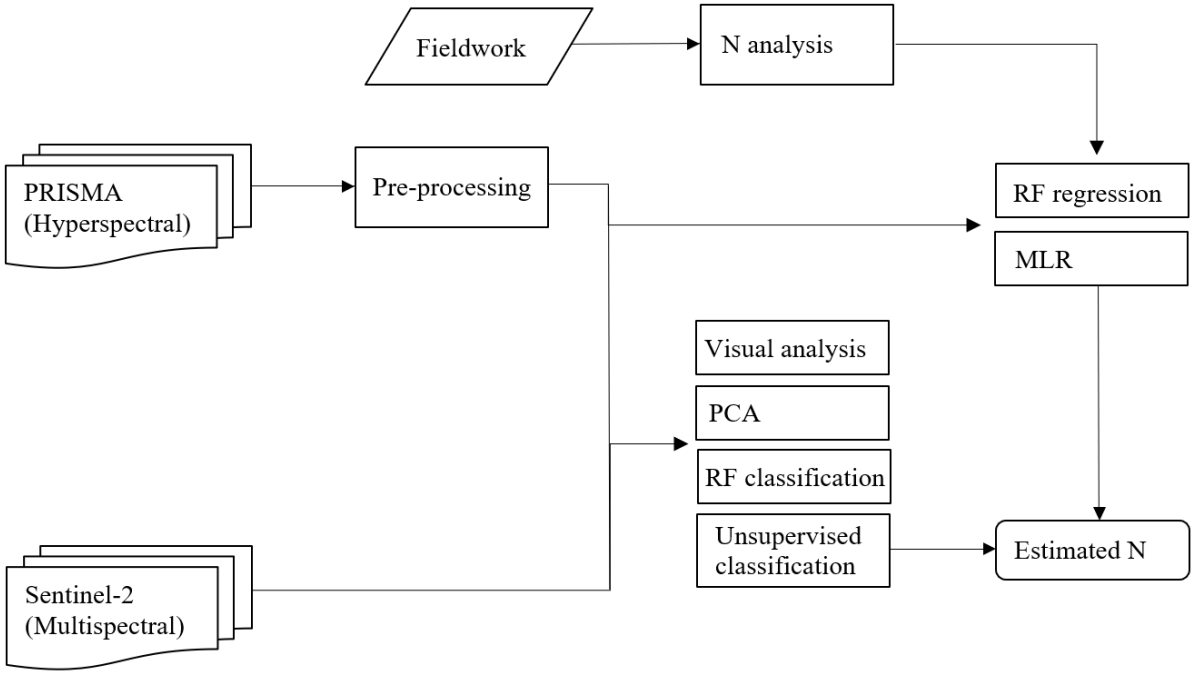

Figure 8. *Flowchart for the project method, where N refers to nitrogen, RF to random forest, and PCA to principal component analysis.*

2.2 Fieldwork

The fieldwork at Långfjället was conducted on the 5th and 6th of August 2022, with supervising help from PhD student Cole Brachmann. Estimations of vegetation cover, GPS points and photographs over the plots were taken on 5 August, and the weather was partly-cloudy. A point frame was used to measure the number of species occurrences, and within each plot, the point frame was used four times (on separate sections of the plot). The resulting species abundance measurements were graciously lent by Brachmann to be used in this project as well.

On 6 August, vegetation samples of the most abundant plant species in the plots were taken. Collectively from all six plots, 24 plant samples of above-ground biomass (leaves and stems) were acquired from the four plants: *Cladonia rangiferina* (Reindeer lichens), *B. nana* (Dwarf birch), *E. hermaphroditum* (Crowberries), and *Calluna vulgaris* (Common heathers). The weather was cloudy with rainfall staring later in the morning. In the field, you could see a clear difference in the vegetation between the exclosures and the ambient plots with an unaided eye. Photographs over two plots show this difference in Figure 9.

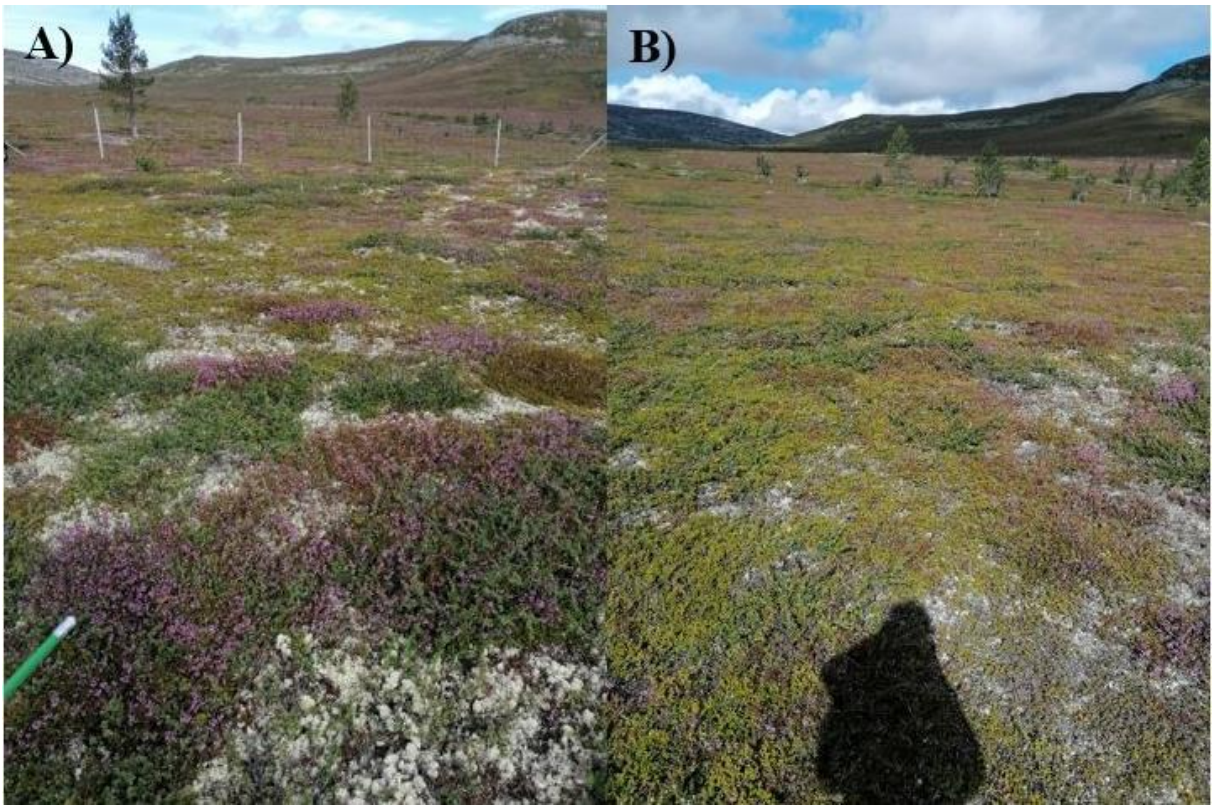

Figure 9. *The two photographs show the difference seen between fenced exclosures (A) vs ambient (B) conditions in field. Both pictures were taken in a north-westerly direction. Photograph A was taken inside plot 1 which is one of the three exclosures, while photograph B was taken in plot 2, which is one of the ambient plots.*

2.3 Nitrogen analysis

A nitrogen analysis was conducted using the vegetation samples from Långfjället. Nitrogen concentrations were estimated through a standard carbon to nitrogen ratio (C/N) analysis using an Isotope-ratio mass spectrometry (IRMS) SerCon 20-22 instrument under the Callisto software and continuous flow IRMS system. The plant samples, taken from the field, were air dried in small paper envelopes and then in the laboratory they were placed inside a drying oven until completely dry (Figure 10a). To grind the plant tissues down into a powder, the plant samples were transferred into test tubes together with small hexagon screw-nuts and then placed in an instrument with high shaking capacity. Preparing for the IRMS, 6 control flour standards (4 ± 0.1 mg) were weighed using a laboratory balance weight and placed in tin capsules (Figure 10b). The same procedure was carried out for the 24 plant samples (2.1 ± 0.1 mg). From the results of the IRMS, the C/N ratio, as well as carbon- and nitrogen amount and isotope ratios were acquired.

Figure 10. *Pictures taken during the nitrogen analysis. Documenting the (a) samples drying in a drying oven and (b) preparation steps before the IRMS when the grounded samples are weighed and placed in tin capsules. Last image, (c) shows all the grinded samples displayed in a row.*

After the results from the IRMS were acquired, t-tests were applied in excel, with the aim to compare exclosures vs ambient plots for the four plant species and their respective N, ^{15}N, C, ^{13}C, and C/N values. Comparisons between these groups were made using unrelated Student's t-test (Equal variance t-test). Student's t-test was selected over Welch's t-test (Unequal variance t-test) as the outcome of three variance tests - The Variance Rule of Thumb, F-test, and Levene's test – pointed in favour of the former. The null hypothesis for each respective plant t-test was that there was no statistical difference in nutrient concentrations between exclosures and ambient plots.

The nitrogen value from the IRMS instrument had to be transformed before it was applied to remote sensing analysis. The plant sample's nitrogen values were weighed against the species abundance measurements (by Brachmann) using the Equation for community weighted average/mean (CWM). Eq 1. from Zeleny (2018) was used to calculate the CWM. The p_{ij} variable from Eq 1. can be calculated using Eq. 2 from Zeleny (2018).

$$c_i = \sum_{j=1}^{S} p_{ij} t_j \quad \text{(Eq. 1)}$$

Where:
S = Is the amounts of plant species measured within the plot.
p_{ij} = The relative prevalence of plant species j.
t_j = Is the "trait" (nitrogen) value for species j.

$$p_{ij} = \frac{I_{ij}}{\sum_{j=1}^{S} I_{ij}} \quad \text{(Eq. 2)}$$

Where:

I_{ij} = Is the prevalence of plant species j. In the equation, I_{ij} is divided by the total abundance for all plant species measured.

2.4 PRISMA Hyperspectral satellite

On the 22nd of March 2019, the remote sensing satellite PRISMA (*PRecursore IperSpettrale della Missione Applicativa*) was launched by the Italian Space Agency (abbreviated from the Italian as ASI) (Loizzo et al., 2019). The payload onboard PRISMA consists of two scientific instruments; a hyperspectral sensor capable of capturing 256 continuous bands in the VNIR - SWIR range (400 – 2500 nm) and a panchromatic camera which can capture one band of medium spectral resolution (400 – 700 nm) (ASI, 2020; Loizzo et al., 2018). The mission goal is to provide further Earth Observation data using a new electro-optical instrument consisting of both hyperspectral and panchromatic technology (Loizzo et al., 2019). The estimated operational lifetime of the PRISMA mission is 5 years (ASI, 2020; Loizzo et al., 2018). The data are freely available after acceptance by ASI of a short scientific proposal.

At a weight of 830 kg, the PRISMA satellite is in the class of small sized spacecrafts (Loizzo et al., 2018; Vangi et al., 2021). PRISMA covers the geographical extent of longitude [180°W to 180°E] and latitude [70°S to 70°N], with a repeat cycle - the time it takes to return to the same location - of 29 days (Loizzo et al., 2019). Each PRISMA image is 30 x 30 km in size and per day PRISMA is capable of obtain up to 223 images (Loizzo et al., 2019). Further technical characteristics of the PRISMA satellite is in *Table 1*. Prisms within PRISMA's hyperspectral instrument act as a dispersing element which captures the incoming radiation and divides it into a 2-D matrix of narrow spectral bands by the across track strip (ASI, 2020). While the 2-D matrix captures the spectral and spatial dimensions, the 'temporal' dimension of the hyperspectral information cube is captured by the satellite as it travels forward in the flight direction (along track) (ASI, 2020). This technique of image capturing is called "Pushbroom" scanning (ASI, 2020; Loizzo et al., 2019).

Table 1. *Technical parameters of PRISMA mission. Based on information and tables in (ASI, 2020; Loizzo et al., 2019; Loizzo et al., 2018).*

Characteristics of PRISMA	
Orbit altitude mean	615 km
Swath/Field of View	30 km / 2.77°
Ground Sampling Distance	Hyperspectral: 30 m Panchromatic: 5 m
Spatial Pixels	Hyperspectral: 1000 Panchromatic: 6000
Spectral Range	VNIR: 400 – 1010 nm (66 bands) SWIR: 920 – 2500 nm (171 bands) PAN: 400 – 700 nm (1 band)
Spectral resolution	≤ 12 nm
Radiometric Quantization	12 bit
Absolute Radiometric Accuracy	Better than 5%
VNIR (Signal-to-Noise Ratio)	> 200:1 for 400 - 1000 nm > 500:1 for 650 nm

SWIR (Signal-to-Noise Ratio)	> 200:1 for 1000 - 1750 nm > 400:1 for 1550 nm > 100:1 for 1950 – 2350 nm > 200:1 for 2100 nm
PAN (Signal-to-Noise Ratio)	> 240:1

2.5 Sentinel-2 multispectral satellite

The Senintel-2 mission of the European Union's Copernicus programme consists of two twin satellites orbiting 180° to each other (Copernicus, 2018; ESA, 2015). The two Sentinel-2 satellites were launched on the 22nd of June 2015 (Sentinel-2A) and the 7th of March 2017 (Sentinel-2B) (Copernicus, 2018). These satellites were constructed by Airbus Defence and Space, but the European Space Agency (ESA) is behind the development (Copernicus, 2018) and is managing the mission (ESA, 2015). Both satellites carry a multispectral instrument called MSI as its payload. The MSI can capture 13 wavelength bands in the range ~ 400-2300 nm with varying spatial resolutions of 10 m, 20 m, and 60 m (*Table 2*). The Sentinel-2 mission operationally covers the geographical extent between latitude 56°S to 84°N (ESA, 2015). With a repeat cycle of 5 days at the equator and up to 3 days at higher latitudes (ESA, 2015). Further information of the Sentinel-2 mission is in *Table 3.*

Table 2. *The information on Senintel-2 mission features is from ESA (2015) and table 1 & 2 from Drusch et al. (2012).*

Features of Sentinel-2 mission	
Orbit altitude mean	786 km
Swath width	290 km
Nr of satellites	2 (180° apart)
Radiometric Quantization	12 bit
Geographic extent	Lat 56°S -84°N
Operational lifetime	7.25 years (batteries and propellants for 12 years)
Satellite weight	~ 1.2 ton

Table 3. *Spectral resolution information for Sentinel-2 MSI. Source for information was taken from the Sentinel-2 image's metadata. In this paper only bands of resolution 10 and 20 m were used in analysis.*

Band	Spatial Resolution [m]	Min wavelength [nm]	Max wavelength [nm]	Central wavelength [nm]
B01 – Coastal aerosol	60	412	456	442,7
B02 – Blue	10	456	533	492,7
B03 – Green	10	538	583	559,8
B04 – Red	10	646	684	664,6
B05 – Red Edge 1	20	695	714	704,1
B06 – Red Edge 2	20	731	749	740,5
B07 – Red Edge 3	20	769	797	782,8
B08 – NIR	10	760	907	832,8
B8A – NIR narrow	20	837	881	864,7
B09 – Water vapor	60	932	958	945,1
B10 – SWIR Cirrus	60	1337	1412	1373,5
B11 – SWIR 1	20	1539	1682	1613,7
B12 – SWIR 2	20	2078	2320	2202,4

2.6 Data for the study

PRISMA and Sentinel-2 images over Långfjället were collected from the PRISMA portal and the Copernicus Open Access Hub respectively. Copernicus Open Access Hub is a free data portal, while PRISMA data are freely available to researchers after an approved application. The images were captured one day apart, on the 21st (Sentinel-2) and on the 22nd (PRISMA) of July 2021. The processing level was L2D for the PRISMA image and L2A for Sentinel-2, meaning that the images are geocoded, atmospherically corrected and measure at-surface reflectance (ESA, 2015; Loizzo et al., 2019). Details of the satellite data used in this study are summarized in Table 4.

Table 4. *Show details of the acquired PRISMA and Sentinel-2 images.*

Data	Date of image (Time of acquisition in parentheses)	Processing level	Accessed from:
PRISMA	2021-07-22 (10:39:12-10:39:19)	L2D	The PRISMA portal http://prisma.asi.it/
Sentinel-2	2021-07-21 (10:40:31)	L2A	Copernicus Open Access Hub https://scihub.copernicus.eu/dhus/#/home

The PRISMA data were not well registered to geographic coordinates. The image was noticeably displaced when compared to Sentinel-2 and orthophotos. Thus, using the software Erdas Imagine, the hyperspectral image was moved 60 m (the equivalent of 2 pixels) towards the west and 120 m (or the equivalent of 4 pixels) southward, so that the two images showed correct geographic alignment.

2.7 PRISMA and Sentinel-2 data analysis

The analyses of the PRISMA and Sentinel-2 data were carried out using various software. These included the programming software MATLAB (which was used to create graphs), Python (Principal component analysis), and R (Machine learning analysis and multiple linear regression). Geographical information systems were used, including QGIS 3.26.3 (including the plugin EnMAP-Box) and ArcMAP, as well as the image processing system ERDAS Imagine.

Besides the manual geo-correction, the hyperspectral PRISMA image was further processed in ERDAS Imagine to improve image quality before further data analysis. For this purpose, the hyperspectral analysis workstation in ERDAS Imagine was used to execute the pre-processing steps. The first step was to identify the wavelength corresponding to the PRISMA bands. Then the next step was to manually remove bad wavelength bands, which is a standard process with hyperspectral data. What is meant by “bad wavelength bands” is unwanted bands which are numerically corrupt (Hexagon Geospatial, 2022). The bands removed were band 56, 103-109, 147-164, and 227-234, corresponding to approximately wavelengths 900 nm, 1350-1420 nm, 1800-1960 nm, and 2450-2500 nm (Figure 11). Hereafter any reference to PRISMA band names in this report will refer to the “bad wavelength band” numbers unless otherwise stated (see Appendix 1, Table 1). Except for original band 56, the PRISMA bands removed correspond to known atmospheric absorption bands and a paper by Liu et al. (2017a) similarly removed wavelength bands in these regions in their method.

The final step in the pre-processing was to use the minimum noise fraction (MNF) tool over the raster to smooth the data and reduce noise, which is also a standard practice with hyperspectral data. Using the method of to fill noise bands with their means and with co-variance skip factor 2. MNF is a type of principal component transform made by Green et al. (1988) and Lee et al. (1990), and is used to order band images after noise level. MNF is used on hyperspectral data, which has varying signal-to-noise ratios (Table 1), to identify noisy bands and then either remove or filter these bands (Hexagon Geospatial, 2022).

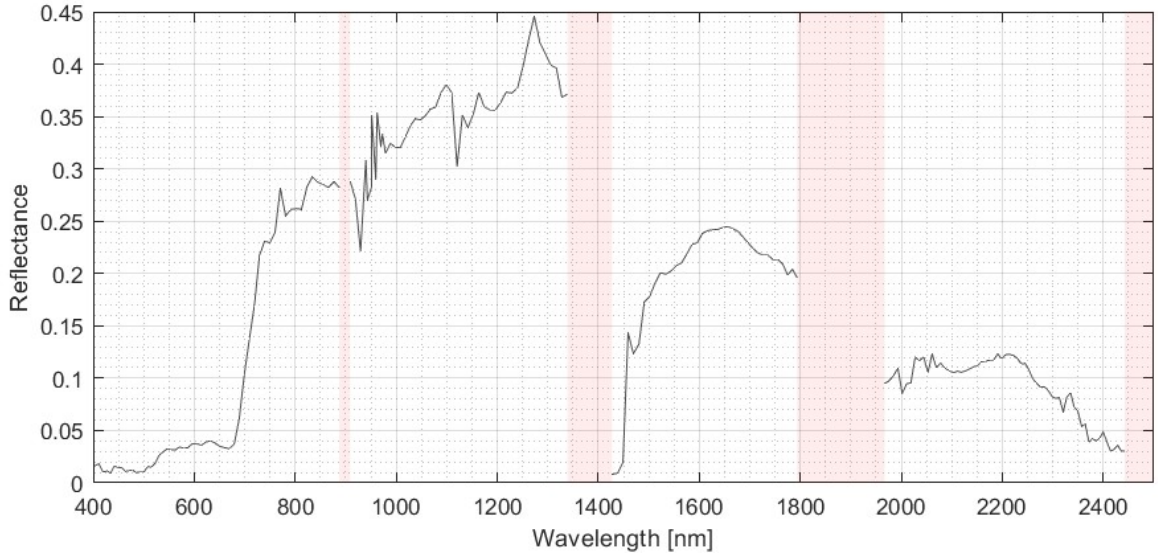

Figure 11. *Illustrates the PRISMA wavelength bands which were removed (shaded in red). The black spectral curve is taken from PRISMA data over Plot 1 (Exclosure).*

After the geometrical correction and pre-processing steps, various methods were employed to answer the research aims. First, a visual comparison of the spectral signature curves from PRISMA and Sentinel-2 over the plots in Långfjället was performed. Using EnMAP-Box spectral library window in QGIS, spectral signature curves for the plots were taken and collected in a spectral library for each satellite. The plots in Långfjället are 25 x 25 m while the hyperspectral PRISMA pixels are slightly larger at 30 x 30 m. One PRISMA pixel per plot, which covered the majority of the plot, was chosen to represent that respective plot (Figure 12). For the multispectral data the Sentinel-2 pixel in the centre of each plot was selected (Figure 12), and the spectral data for each band was extracted. Lastly, graphs for all spectral curves collected were plotted in MATLAB.

A principal component analysis (PCA) of the hyperspectral image was conducted with the aim of discerning which wavelength bands contribute most to the variability of the original hyperspectral data. This was done in Python using solely data over the six plots in Långfjället. Partial least squares regression (PLSR), random forest (RF) regression and classification were attempted for both the hyperspectral and multispectral datasets in programming software R. Variable importance for a RF regression is evaluated through a measure called the percent increase in mean squared error, or "%IncMSE" (Freeman et al., 2016), while variable importance of a RF classification can be measured through the function "VarSelRF" (Diaz-Uriarte, 2007).

If there is a small sample size used for training data, machine learning algorithms, such as RF and PLSR, can be more susceptible to overfitting, this is known as the "curse of dimensionality" (Belgiu & Drăguţ, 2016; Ghosh et al., 2014). Overfitting is a process where a trained model learns the training data too well, to the point where it performs poorly on new test data (Montesinos López et al., 2022). A simple parametric multiple linear regression (MLR) was instead applied in succession for each respective wavelength band, for both the hyperspectral and multispectral datasets, in the statistical software R. Two linear regressions were run (one for exclosures and one for ambient plots) for each band, against the nitrogen CWM. The resulting R2 values were used to compare significance.

Because regression equations to estimate nitrogen were created separately for the exclosures and ambient areas, to create a map of nitrogen over the satellite image it first required classifying these two types of vegetation. This was done using an unsupervised classification in ERDAS Imagine on a subset of the pre-processed PRISMA image. An unsupervised classification was chosen as a method because it can be performed when there is little to no field data to be used as training data (Campbell et al., 2022). Bands selected for the unsupervised classification were primarily based on RF classification variable selection result, i.e., the "VarSelRF" result. The resulting unsupervised classification was then manually grouped into exclosure vs ambient pixels. Then the linear functions from the MLR was applied using the classified raster as a mask.

Figure 12. *Displays which pixels were selected to represent the plots from the PRISMA (left) and Sentinel-2 data (right). For PRISMA the pixel with most area within the respective plots was selected to represent that plot. These cells are marked with black crosses in the map (left). For Sentinel-2 the centre pixels were selected, also shown as smaller black crosses in the map (right). The maps display 'True color' for PRISMA (30 m resolution) and Sentinel-2 (10 m resolution).*

3. Result

3.1 Nitrogen results

A nitrogen analysis was carried out for the four most abundant plant species in Långfjället. The IRMS gave N, ^{15}N, C, ^{13}C, and C/N values for each of the 24 collected plant samples. From the IRMS results, the lichen sample from ambient Plot 6 showed much larger concentrations in comparison to other plots' lichen samples. So the decision was made to exclude these values from Plot 6. Table 5 displays a summary of the results obtained from the IRMS analysis. From the nitrogen concentration means in Table 5, it is clear that *Cladonia rangiferina* has much lower mean nitrogen values than either *E. hermaphroditum*, *B. nana*, or *Calluna vulgaris*. Specifically, nitrogen values from the *Cladonia rangiferina* samples are only approximately 40 % of the concentrations measured for *E. hermaphroditum* or *Calluna vulgaris*, and only 20 % compared to *B. nana.* Another interesting difference between *Cladonia rangiferina* and the other vegetation species is highlighted by the C/N means. The *Cladonia rangiferina* C/N mean is about twice that of *E. hermaphroditum* or *Calluna vulgaris,* while *B. nana* is closer to having a C/N mean equivalent to only one-fifth to one-quarter that of *Cladonia rangiferina.* From the table we can also see that *B. nana* has by far the highest ^{15}N means.

Table 5. *Result from the IRMS analysis.*

		Mean				
		N (%) [a]	δ^{15}N (‰) [a]	C (%) [b]	δ^{13}C (‰) [b]	C/N
Empetrum hermaphroditum	Exclosure	0,95	-5,44	54,11	-26,71	57,11
	Ambient	0,81	-8,39	53,94	-27,37	66,62
Betula nana	Exclosure	1,67	-0,54	50,95	-29,10	31,56
	Ambient	1,90	-0,49	50,18	-29,42	26,83
Calluna vulgaris	Exclosure	1,03	-3,74	51,22	-28,78	49,90
	Ambient	0,97	-5,23	50,91	-28,83	52,74
Cladonia rangiferina	Exclosure	0,38	-5,49	43,27	-25,77	119,95
	Ambient	0,33*	-6,86*	42,59*	-26,43*	130,29*

Note. * One ambient plot (Plot 6) was excluded as a precaution from mean calculation because the IRMS results for this sample looked odd.

[a] Standards were measured against atmospheric nitrogen ratio (Sercon, 2018).

[b] Standards were measured against Pee Dee Belemnite (PDB) ratio (Sercon, 2018).

Tables 6 & 7, show the results from the Student's t-tests for N, ^{15}N, and C/N. From these tables it is apparent that only *E. hermaphroditum* shows statistically significant p-values for all three factors: N, ^{15}N, and C/N. Additionally, only the t-test for ^{15}N yielded another statistically significant p-value for *Calluna vulgaris.* Unexpectedly, no other significant difference between exclosures and ambient plot was found. It is possible that the sample size was too small to investigate the difference in the environmental conditions.

Table 6. *Student's t-test results for N and ^{15}N in differentiating between exclosures vs ambient plots, by vegetation type. In the graph: SE = Standard error, t=t-score, df=degrees of freedom, and P=p-value.*

	N					^{15}N				
	Mean (%)	SE (%)	t	df	P	Mean (‰)	SE (‰)	t	df	P
Empetrum hermaphroditum										
Exclosure	0,95	0,02				-5,44	0,22			
vs			3,07	4	0,04*			4,51	4	0,01*
Ambient	0,81	0,04				-8,39	0,62			
Betula nana										
Exclosure	1,67	0,23				-0,54	0,77			
vs			-0,83	4	0,45			-0,02	4	0,99
Ambient	1,90	0,15				-0,49	2,51			
Calluna vulgaris										
Exclosure	1,03	0,03				-3,74	0,41			
vs			0,87	4	0,44			3,53	4	0,02*
Ambient	0,97	0,06				-5,23	0,11			
Cladonia rangiferina										
Exclosure	0,38	0,05				-5,49	1,09			
vs			0,69	3	0,54			0,97	3	0,40
Ambient	0,33	0,02				-6,86	0,27			

Note. * Statistically significant p-value

Table 7. *Student's t-test results for C/N in differentiating between exclosures vs ambient plots, by vegetation type. In the graph: SE = Standard error, t=t-score, df=degrees of freedom, and P=p-value.*

	C/N				
	Mean	SE	t	df	P
Empetrum hermaphroditum					
Exclosure	57,11	0,51			
vs			-3,70	4	0,02*
Ambient	66,62	2,52			
Betula nana					
Exclosure	31,59	3,75			
vs			1,07	4	0,34
Ambient	26,83	2,31			
Calluna vulgaris					
Exclosure	49,90	2,42			
vs			-0,74	4	0,50
Ambient	52,74	2,96			
Cladonia rangiferina					
Exclosure	119,95	17,48			
vs			-0,44	3	0,69
Ambient	130,29	9,06			

Note. * Statistically significant p-value

The CWM, or the nitrogen values from the IRMS weighed against the species abundance measurements, are presented in Table 8. There are not any discernible patterns when comparing exclosures versus ambient plots for *E. hermaphroditum* and *B. nana*, nor for the summary CWM. However, CWM of nitrogen for *Calluna vulgaris* shows a clear difference as all exclosed plots have lower CWMs while all ambient plots have higher CWMs. Regarding *Cladonia rangiferina*, since plot 6 is excluded it is even harder to compare exclosures versus ambient plots. There appears to be a tendency for *Cladonia rangiferina* exclosures to have higher CWMs of nitrogen than the ambient plots. As previously mentioned, the small sample size hinders further analysis.

Table 8. *The CWM of nitrogen in the table is based on a vegetation inventory by Cole Brachmann and on the nitrogen amount from the IRMS analysis. Fenced exclosures are odd numbers and shaded. Ambient plots are even plot numbers and have white background.*

	Empetrum hermaphroditum (%)	*Betula nana* (%)	*Calluna vulgaris* (%)	*Cladonia rangiferina* (%)	***SUM* (%)**
Plot 1	0,30	0,35	0,07	0,13	0,85
Plot 2	0,35	0,28	0,16	0,09	0,87
Plot 3	0,42	0,42	0,05	0,09	0,98
Plot 4	0,27	0,24	0,33	0,07	0,91
Plot 5	0,25	0,19	0,06	0,25	0,75
Plot 6	0,21	0,59	0,12	-*	0,92

Note. * This value is excluded from the results because the nitrogen amount from the IRMS analysis for this sample was believed to be unreliable.

3.2 Hyperspectral vs Multispectral

A visual comparison of the spectral curves from PRISMA hyperspectral data against Sentinel-2 multispectral data for exclosures vs ambient plots in Långfjället was carried out. Figure 13 shows solely the PRISMA spectral data, while Figure 14 presents the spectral curves from Sentinel-2. What stands out from both figures, despite the difference in spectral resolution between the two sensors, is that the spectral curves over the ambient plots tend to have lower reflectance than the exclosures.

Figure 15 shows the combined PRISMA and Sentinel-2 spectral curves. The largest difference between the two satellites is in the VIS range, though a disparity can also be observed over Sentinel-2 points in the NIR spectrum. Note however that the Sentinel-2 spectral data have higher reflectance than PRISMA in the VIS range, while it is the opposite in the NIR range where Sentinel-2 reflectance is lower. It can also be seen from Figure 15 that the Sentinel-2 reflectance is slightly lower in the first SWIR peak. These two spectral images were acquired one day apart, towards the end of July 2021 and during the same time of day.

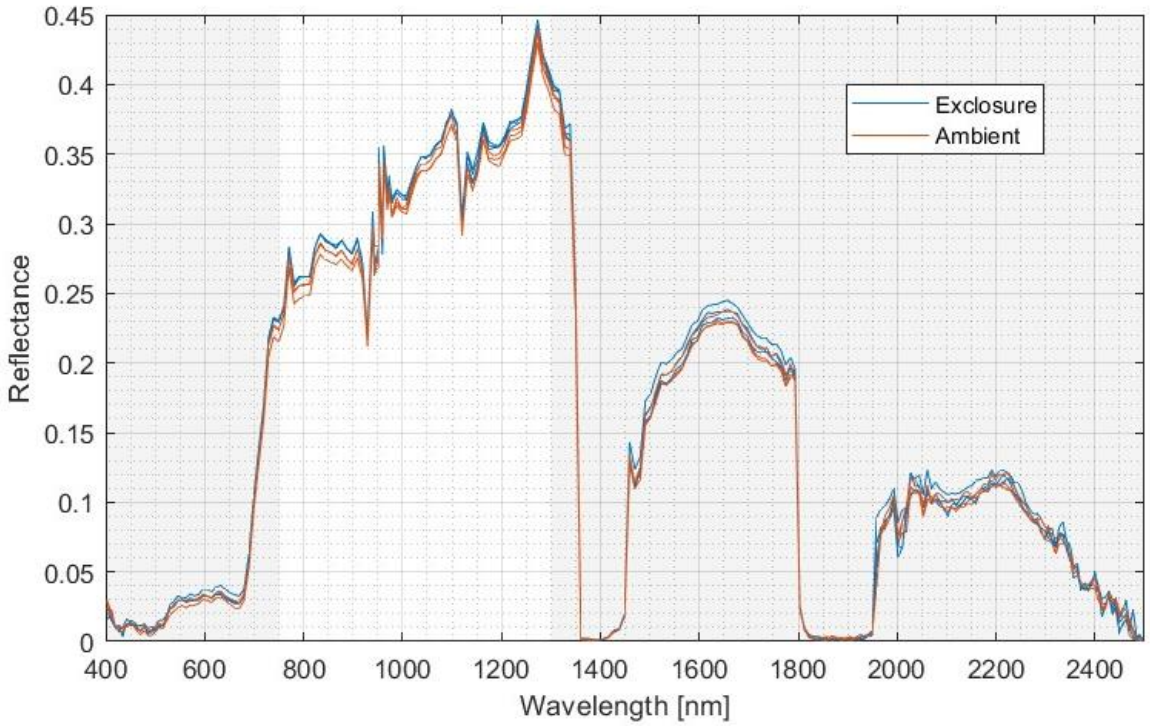

Figure 13. *Spectral signature curves for hyperspectral PRISMA data. The three exclosures are drawn as blue lines while the three ambient plots are displayed in red.*

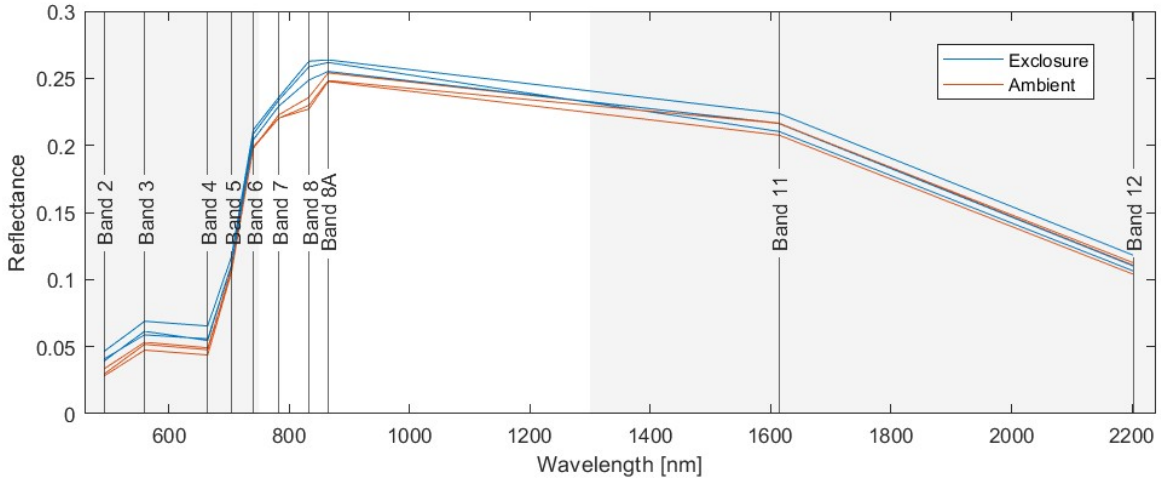

Figure 14. *Presents spectral curves for multispectral Sentinel-2 data. Only bands with resolution of 10 m or 20 m where included. The three exclosure plots are shown as blue lines while the three ambient plots are drawn in red.*

Looking at Figure 16, 17, & 18, we see a closer view of the VIS, NIR, and SWIR regions respectively from Figure 15. At this scale it is evident that the largest difference between PRISMA and Sentinel-2 data occurs in the VIS part of the spectrum prior to the red edge (Figure 16). Additionally, Sentinel-2 bands B02, B03, and B04, display a clear difference between exclosures and ambient plots that is not mirrored with the PRISMA bands, which are more intertwined. Sentinel-2 only has bands in the shorter wavelengths of the NIR spectrum, and here as well there is a clear division between exclosures and ambient plots. However, this division is also visible for PRISMA bands over the same spectrum (Figure 17). While for the SWIR range, even at a closer view, no noticeable difference between exclosures and ambient plots can be observed for either satellite (Figure 18).

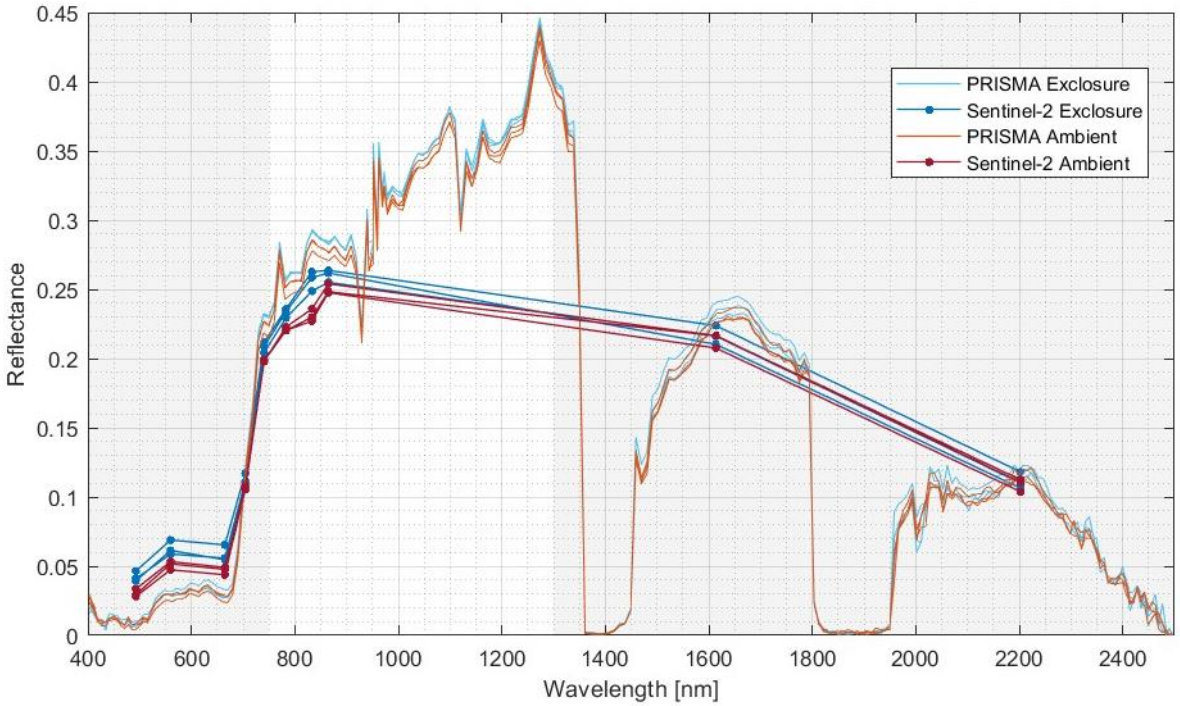

Figure 15. *Displays the spectral curves for both PRISMA and Sentinel-2. The three exclosures are drawn in blue, with PRISMA in a lighter hue and Sentinel-2 in a darker blue. Whereas the three control plots are displayed in red shades, PRISMA in a lighter orange-red colour and Sentinel-2 in a dark red colour.*

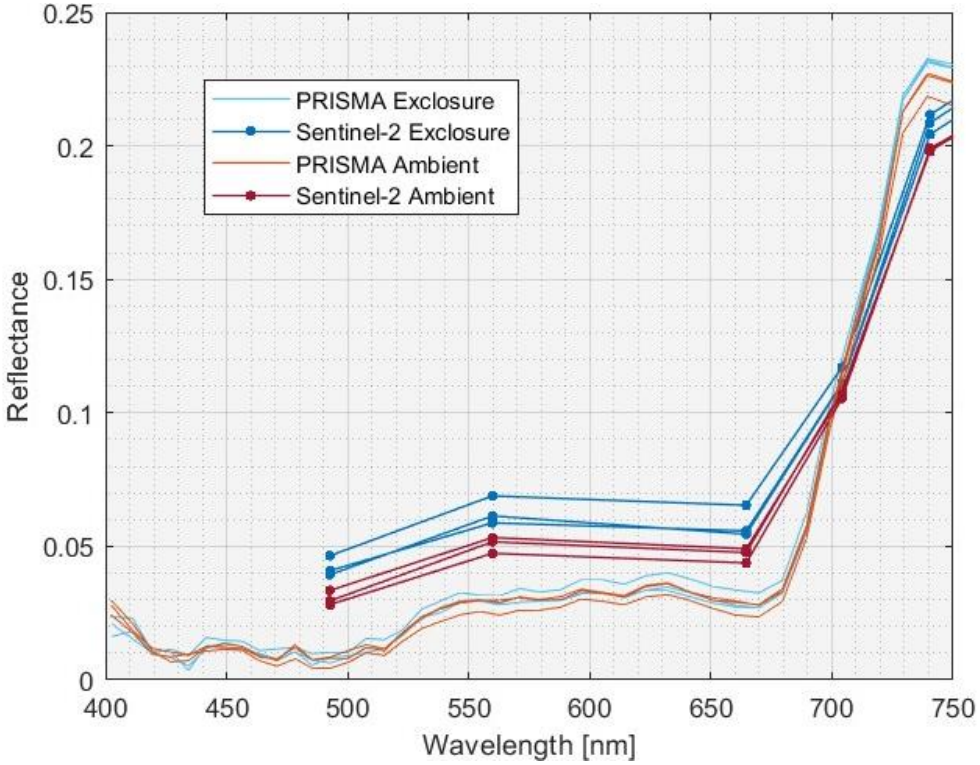

Figure 16. *Zoom in on the VIS spectrum showing the spectral curves for both PRISMA and Sentinel-2. The three exclosures are drawn in blue, with PRISMA in a lighter and Sentinel-2 in a darker blue. While for the three control plots, PRISMA is shown in a lighter orange-red colour and Sentinel-2 in a dark red colour.*

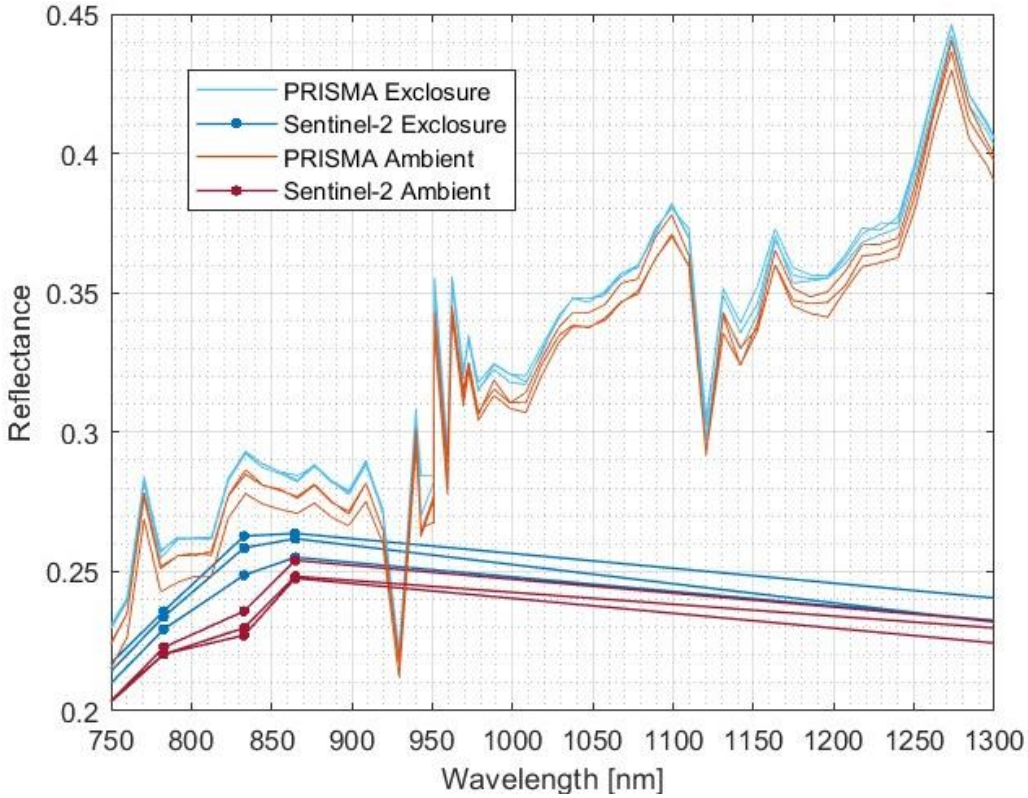

Figure 17. *Zoom in on the NIR spectrum with spectral signature curves for both PRISMA and Sentinel-2. The three exclosures are drawn in blue, with PRISMA in a lighter hue and Sentinel-2 in a darker blue. Whereas the three control plots are displayed in red shades, PRISMA in a lighter orange-red colour and Sentinel-2 in a dark red colour.*

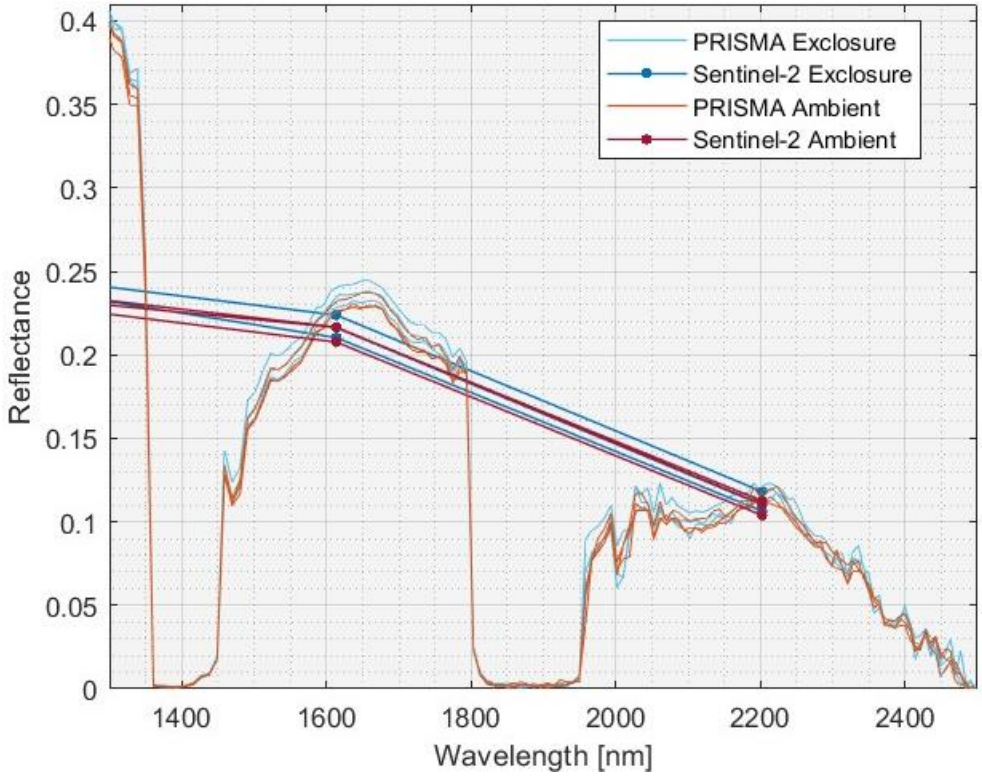

Figure 18. *Zoom in on the SWIR range showing the spectral curves for both PRISMA and Sentinel-2. The three exclosures are drawn in blue, with PRISMA in a lighter hue and Sentinel-2 in a darker blue. Whereas the three control plots are displayed in red shades, PRISMA in a lighter orange-red colour and Sentinel-2 in a dark red colour.*

Looking at Figure 19 & 20, further details are presented about the exclosures and ambient plots respectively. In Figure 19, looking at only exclosures, it appears that Plot 1 has higher reflectance than the other exclosures. Whereas in Figure 20, a graph which only has ambient plots, it seems like Plot 4 has the lowest reflectance among the ambient plots.

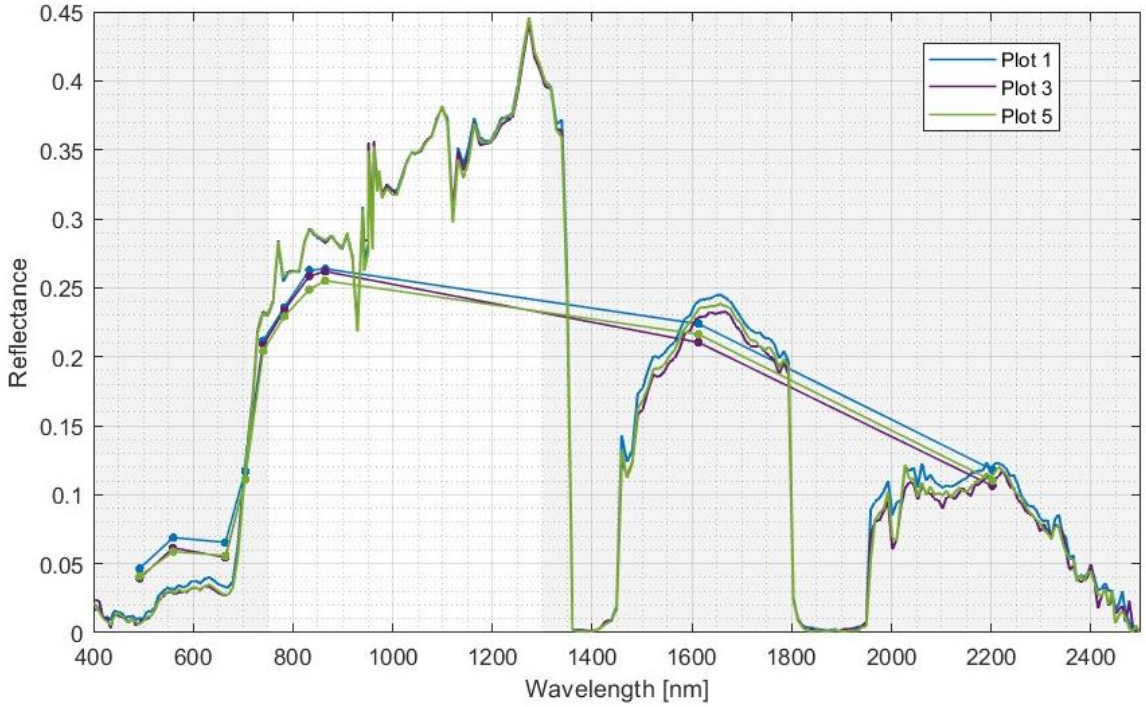

Figure 19. *Shows only the spectral curves taken from exclosures, i.e., Plot 1, Plot 3, and Plot 5. Both PRISMA and Sentinel-2 share matching colour coding in the graph, Plot 1 is displayed in blue, Plot 3 in purple, and Plot 5 in green.*

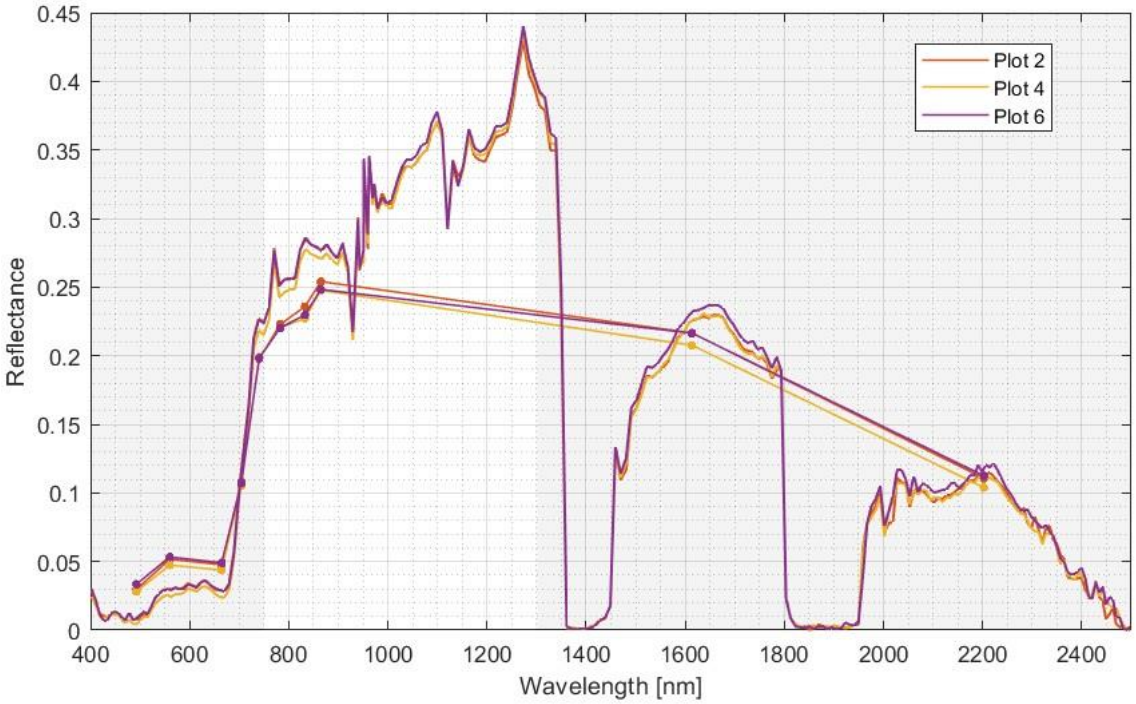

Figure 20. *Graph of only spectral curves taken from ambient plots, i.e., Plot 2, Plot 4, and Plot 6. Both PRISMA and Sentinel-2 share matching colour coding in the graph, Plot 2 is displayed in red, Plot 4 in yellow, and Plot 6 in purple.*

3.3 Principal Component Analysis

A PCA analysis using all post-processed bands of PRISMA spectral data from the six plots was carried out. In Figure 21, we see the plots (exclosures in blue and ambient in red) scattered on PC 1 vs PC 2. The optimal result would be if the two different traits formed two distinct clusters. Instead, in Figure 21, it appears that the fenced exclosure plots are dissimilar. This also appears to be the case in Appendix 2, Figure 1, 2, & 3, where the CWM of nitrogen for each plot is scattered against PC 1, PC2 and the fraction of PC2/PC1 respectively.

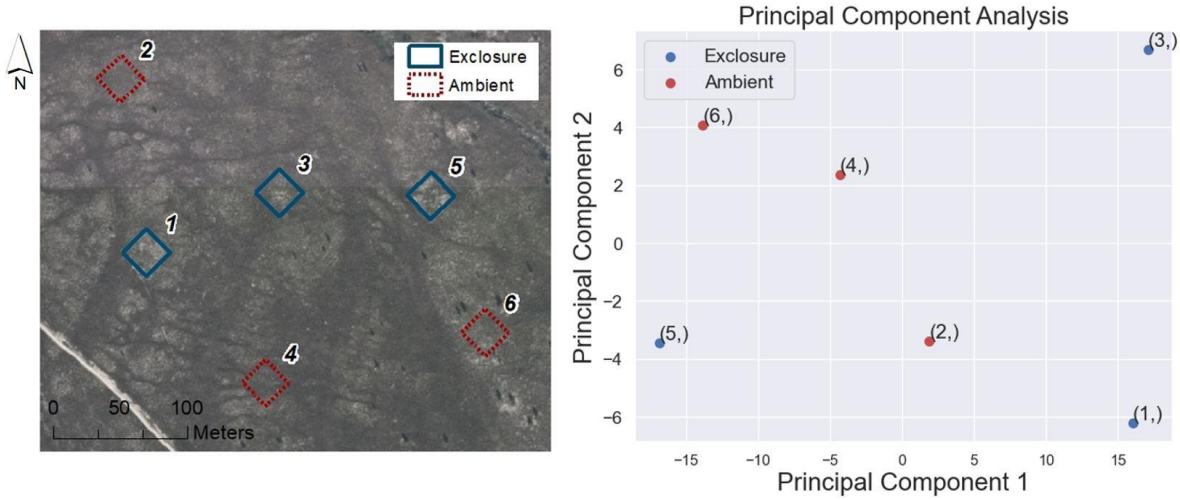

Figure 21. *A scatter plot of PC 1 against PC 2 is shown on the right and a map of the location of the six plots to the left. Exclosure plots and points are in blue and ambient in red.*

Together PC 1 and PC 2 explain over 95 % of variance of the original data, Figure 22. While in the correlation matrix in Figure 23, PC 1 correlates most to PRISMA bands 110 – 130 (~ 1510 – 1640 nm), while PC 2 correlates to bands 2 – 4 (~ 410 – 430 nm). In Figure 23, besides having highest correlation to bands 110 – 130, PC 1 appears to correlate to bands 36-38, 105 – 138 and 146 – 185. In contrast PC 2, which seems to have high correlation only to the narrow wavelength bands around bands 2 – 4.

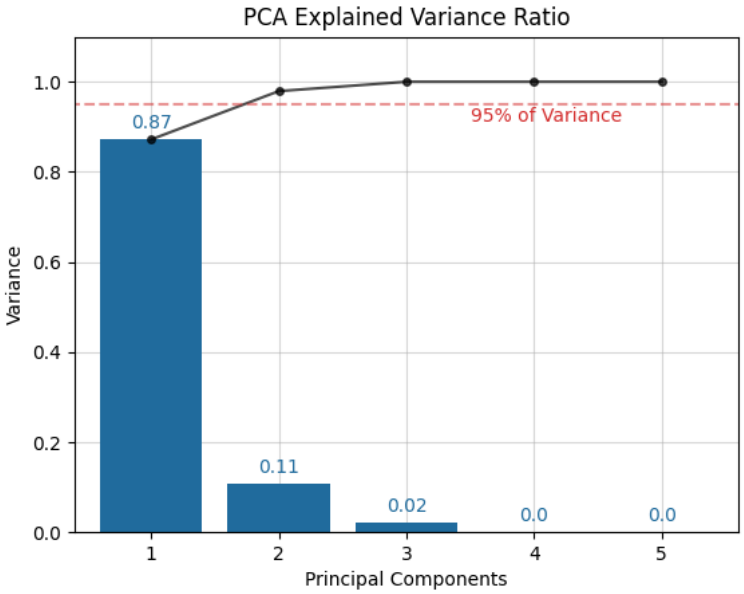

Figure 22. *Presents how much each principal component contributes to explain the variation in the original dataset.*

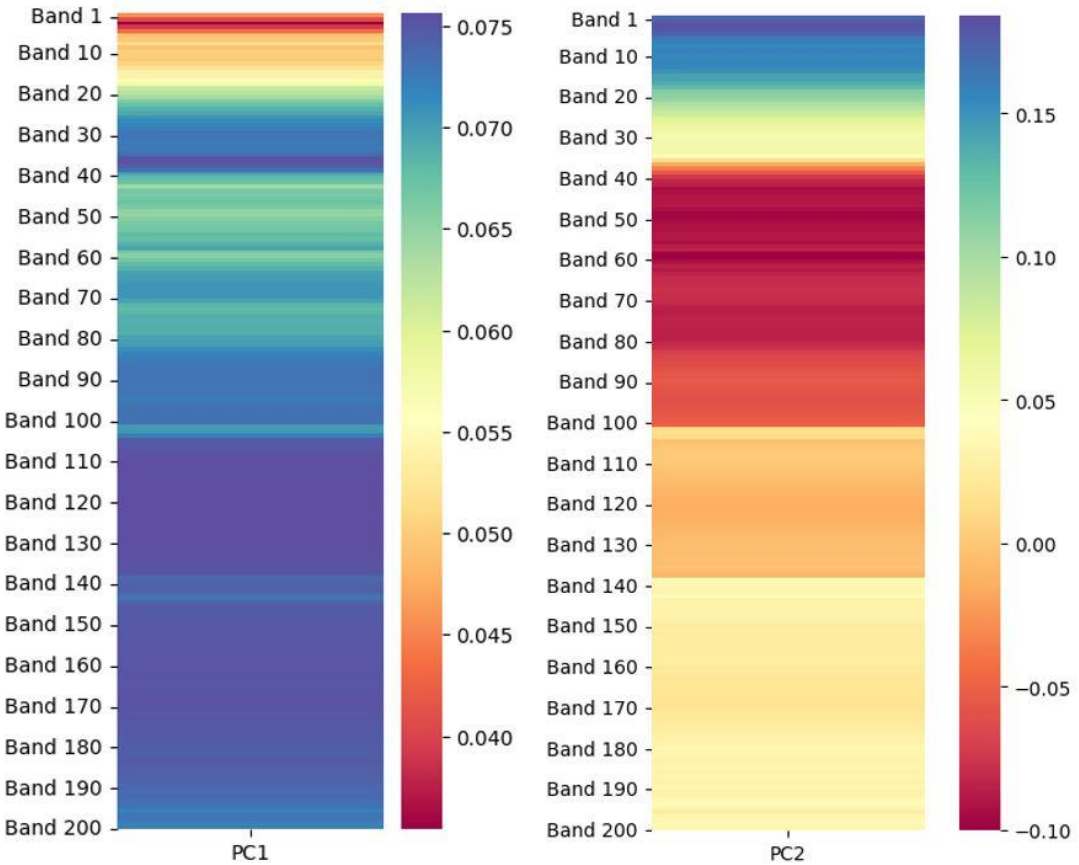

Figure 23. *Correlation matrix of PRISMA bands against PC 1 (the figure to the left) and PC 2 (the figure to the right).*

3.4 Random Forest

Both a RF regression and classification was carried out for the PRISMA and Sentinel-2 plot data. The small size of the field data collected meant that the attempted analyses -- partial least squares regression (PLSR), random forest (RF) regression and classification -- gave unreliable results. The RF regression for both PRISMA and Sentinel-2 data gave a result (see Appendix

3, Figure 1) with low percent of variance explained ("% var explained"). The variable importance of each band is evaluated through "%IncMSE" in R's RF regression. In Figure 24 the PRISMA the percent increased in "%IncMSE", or in other terms the bands most important for the regression, is shown. A RF classification for both PRISMA and Sentinel-2 data was also executed, see Appendix 3. With out-of-box errors of 33.33 % for PRISMA respectively 0 % for Sentinel-2. A RF R function called "VarSelRF" was used to select bands with most importance for PRISMA (Figure 25) and Sentinel-2 (Table 9).

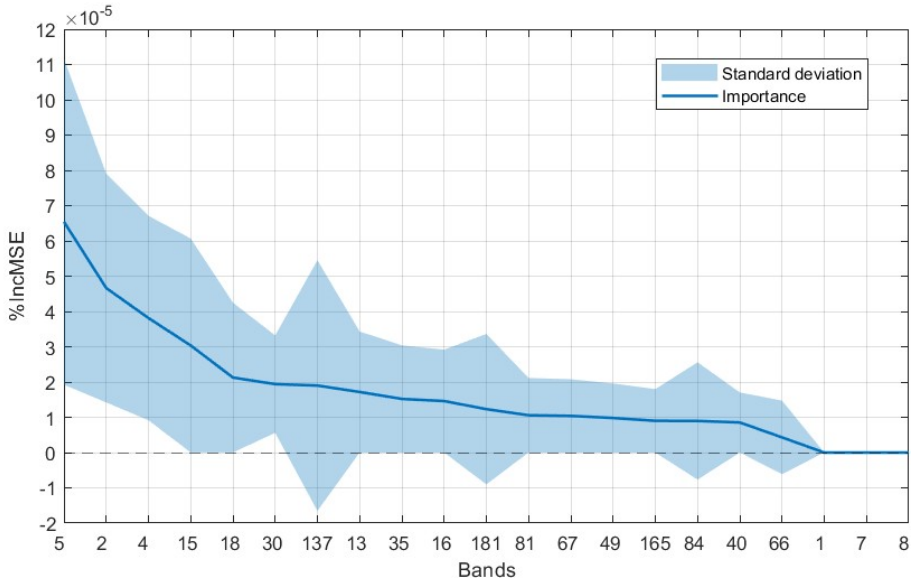

Figure 24. *Showing improvement (positive %IncMSE) gained when adding specific bands for the RF regression between N and PRISMA data. X-axis shows the specific PRISMA band number.*

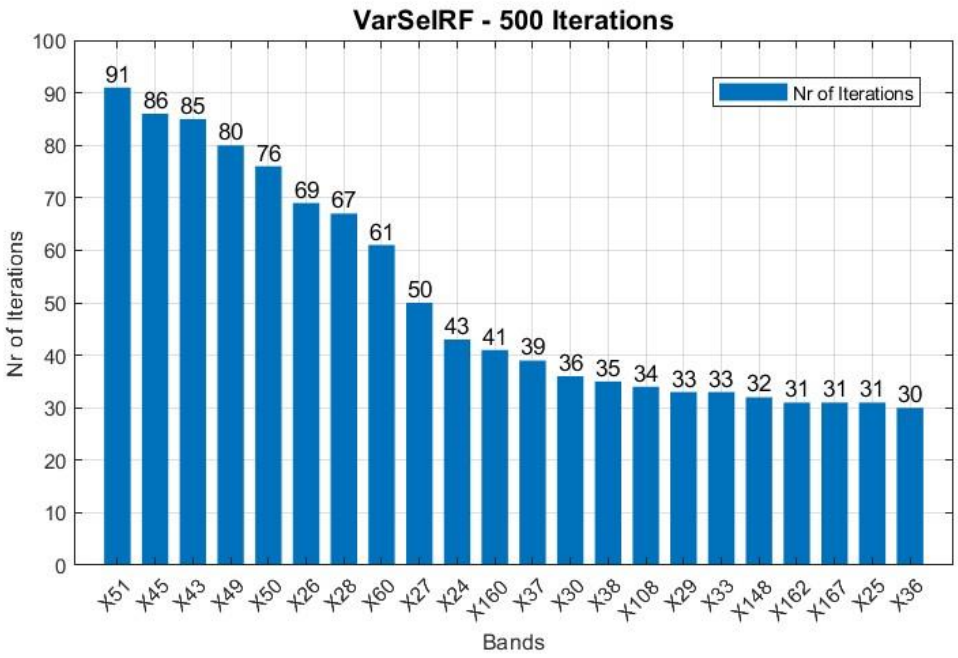

Figure 25. *The R function VarSelRF was repeated 500 times in a loop. The X-axis shows the bands that were most important in the regression function for estimating nitrogen from PRISMA data. The bands on the X-axis show increasing importance from left to right. The number above the bar indicates the number of times that the band was found to be important in the 500 iterations. For example, Band 51 was most often an explanative variable in the multiple iterations.*

Table 9. *VarSelRF (repeated for 100 loops) for Sentinel-2. Bands with higher occurrences from VarSelRF are deemed to be more important.*

Sentinel-2 band (20 m)	VarSelRF (100 iterations)
B05	100
B07	96
B03	77
B06	64
B02	27
B04	12
B8A	12
B11	8
B12	8

3.5 Multiple Linear Regression

MLR was performed on each individual PRISMA band against the CWM of nitrogen. For each function, two linear regression lines were calculated from the predictors: exclosures vs ambient plots. To compare the regressions from each wavelength band, the coefficient of determination, i.e., R2, was used as it gives an indication of the how well each wavelength band predicted the dependent variable (the CWM of nitrogen). In Figure 26, the R2 values for all the PRISMA wavelength bands are displayed. Wavelength bands below band 35 (~680 nm), i.e., the VIS, have the highest observed R2 values, while the NIR range from around band 40 (~730 nm) to band 100 (~1330 nm) have the lowest R2 values and least explain the dependent variable. All the highest observed R2 values, above R2=0.7, from the MLRs are shown in Figure 27. In the figure we can see that while all R2 values >0.7 are below ~680 nm (band 35), all bands with an R2 >0.8 are under ~610 nm (band 28).

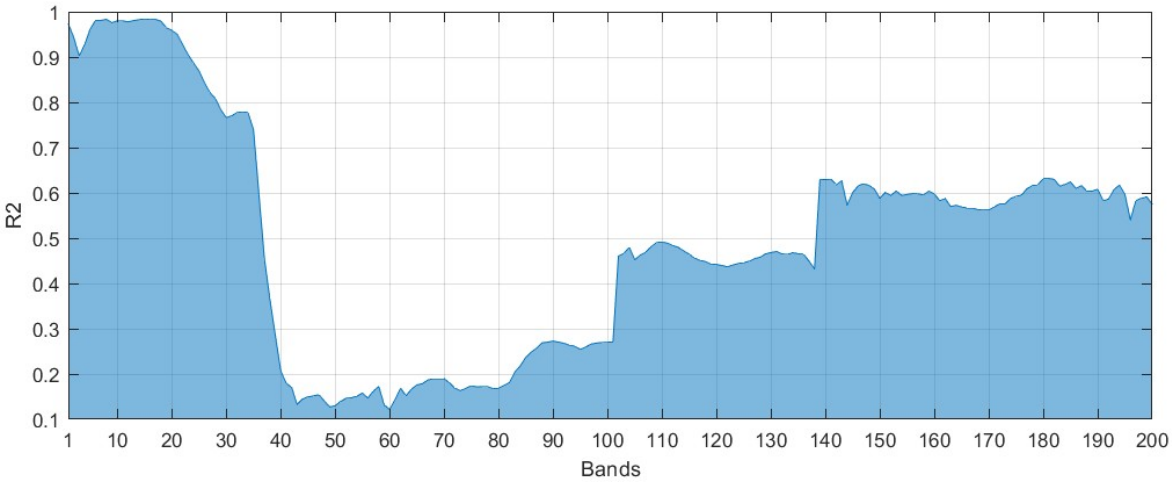

Figure 26. *Presents an overview of R2 values from MLR for all PRISMA Bands.*

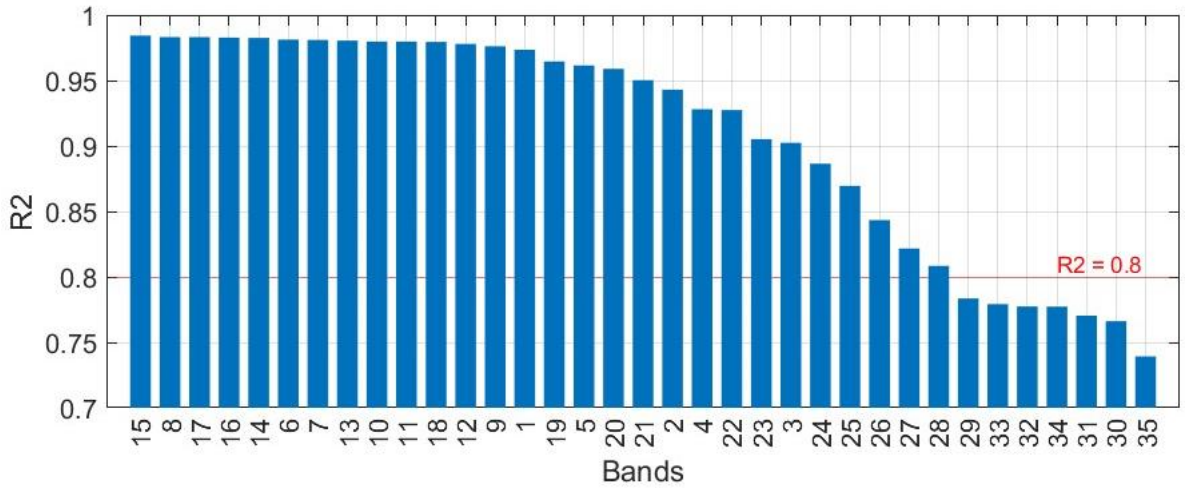

Figure 27. *Display all PRISMA bands with a MLR R2 value above 0.7, in order of decreasing value.*

MLR was also carried out for the Sentinel-2 bands, for both bands in resolution 10 m and 20 m. The resulting R2 from the Sentinel-2 MLR yielded much lower values than for the PRISMA bands, Table 10. The Sentinel-2 R2 values are comparable to the lowest R2 values in the NIR regions for the PRISMA wavelength bands. The bands with the highest R2 are B08 (for 10 m) and B02 (for 20 m).

Table 10. *Shows the R2 result from MLR for Sentinel-2 bands of resolution 10 m and 20 m.*

Sentinel-2 (10 m)		Sentinel-2 (20 m)	
Bands	*R2*	*Bands*	*R2*
B02	0,13	B02	0,35
B03	0,09	B03	0,17
B04	0,08	B04	0,21
B08	0,36	B05	0,09
		B06	0,15
		B07	0,24
		B8A	0,26
		B11	0,20
		B12	0,16

In Figure 28, the linear regression lines for PRISMA band 1 are presented. The linear regression formula for exclosures is $y = 0.0016x - 2.0015$ with R2 = 0.98, while the linear regression formula for ambient plots is $y = 0.0012x - 1.2805$ with R2 = 0.89. From the relative position of the respective regression functions it appears that the exclosures have lower nitrogen content.

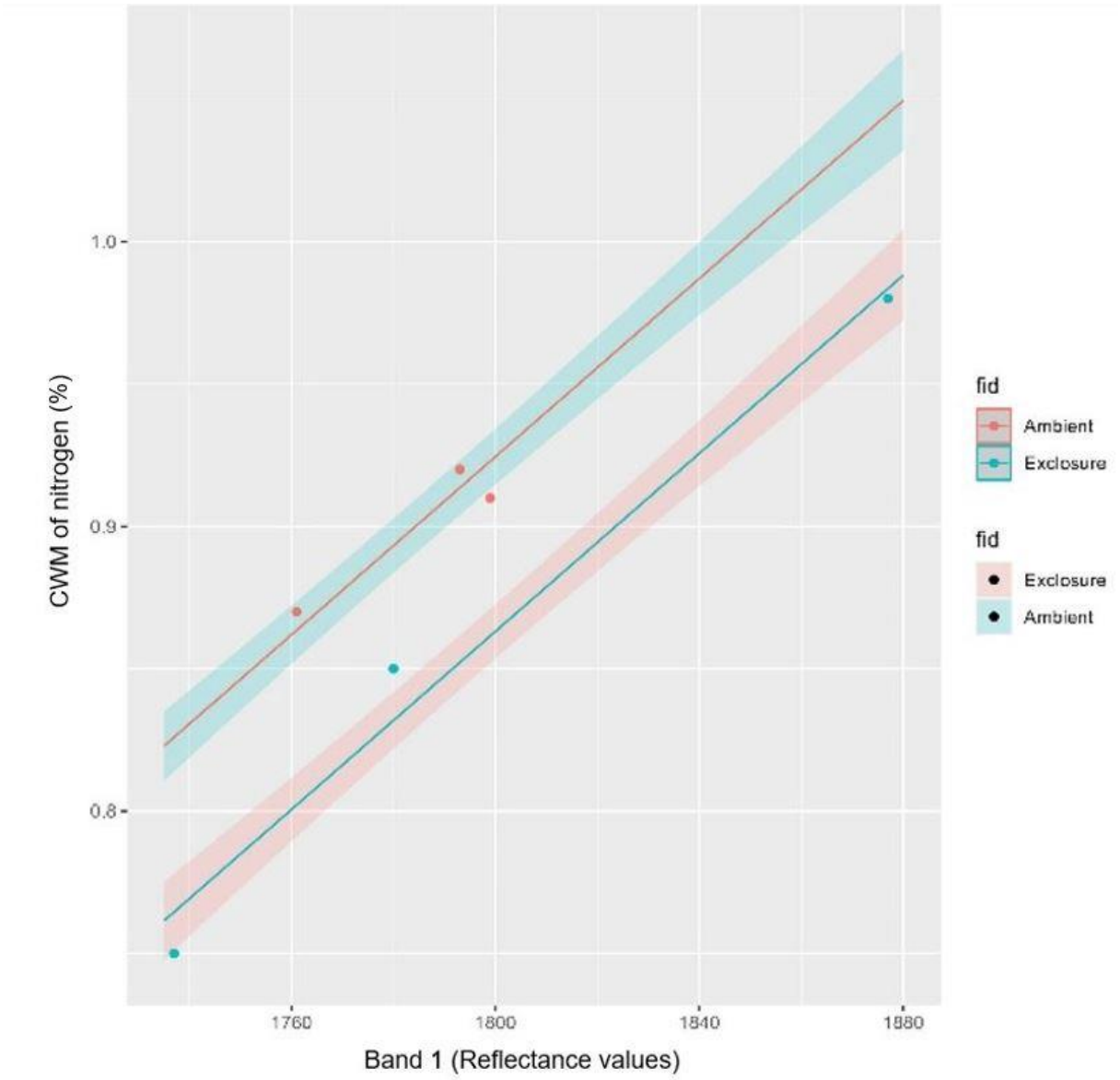

Figure 28. *Shows the MLR for band 1 against the CMW of nitrogen. The six points represent the plots from Långfjället. Band 1 had an R2 value of approximately 0.97.*

3.6 Unsupervised Classification and Estimation of Nitrogen

An unsupervised classification of a subset of the PRISMA raster was carried out using only the selected bands: 1, 26, 37, 45, 51, 60, 108, 131, & 160 (approximately 400 nm, 600 nm, 700 nm, 780 nm, 840 nm, 940 nm, 1490 nm, 1730 nm, & 2140 nm respectively). Figure 29 illustrates the placement of the selected bands in relation to the spectral curves for the six plots. The linear regression functions from the MLR of band 1 were then applied on the classified raster to estimate nitrogen content. The resulting maps of both the unsupervised classification and the estimated nitrogen values can be seen in Figure 30.

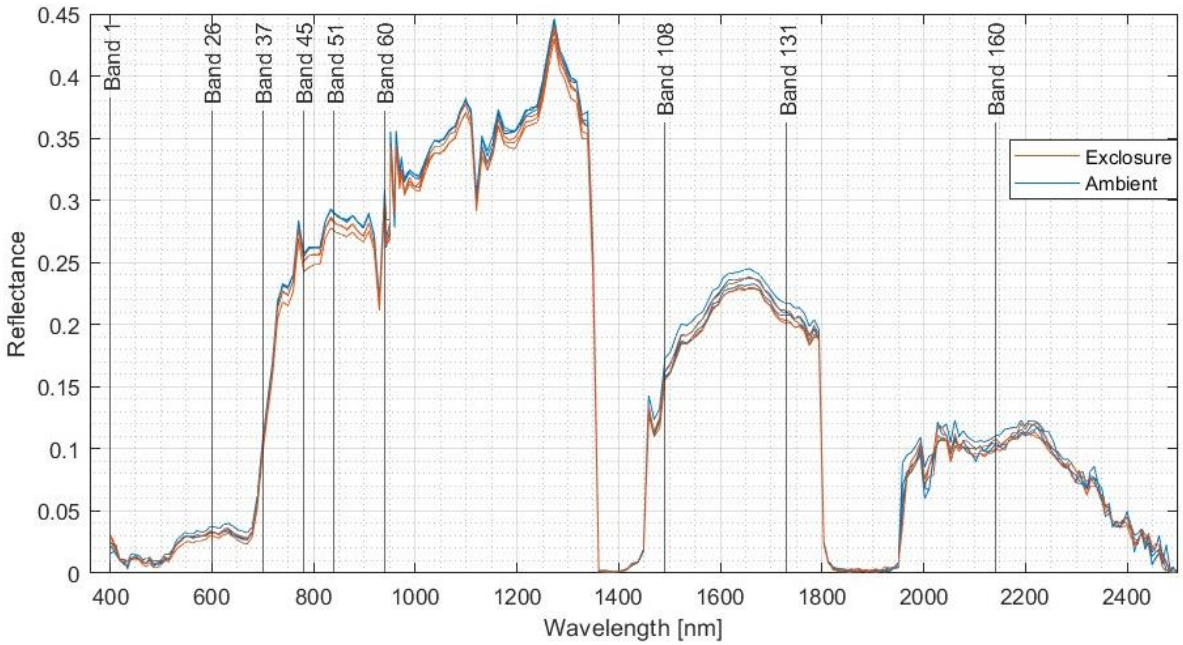

Figure 29. *Show the location of the bands selected for the unsupervised classification on the PRISMA spectral curves of the six plots.*

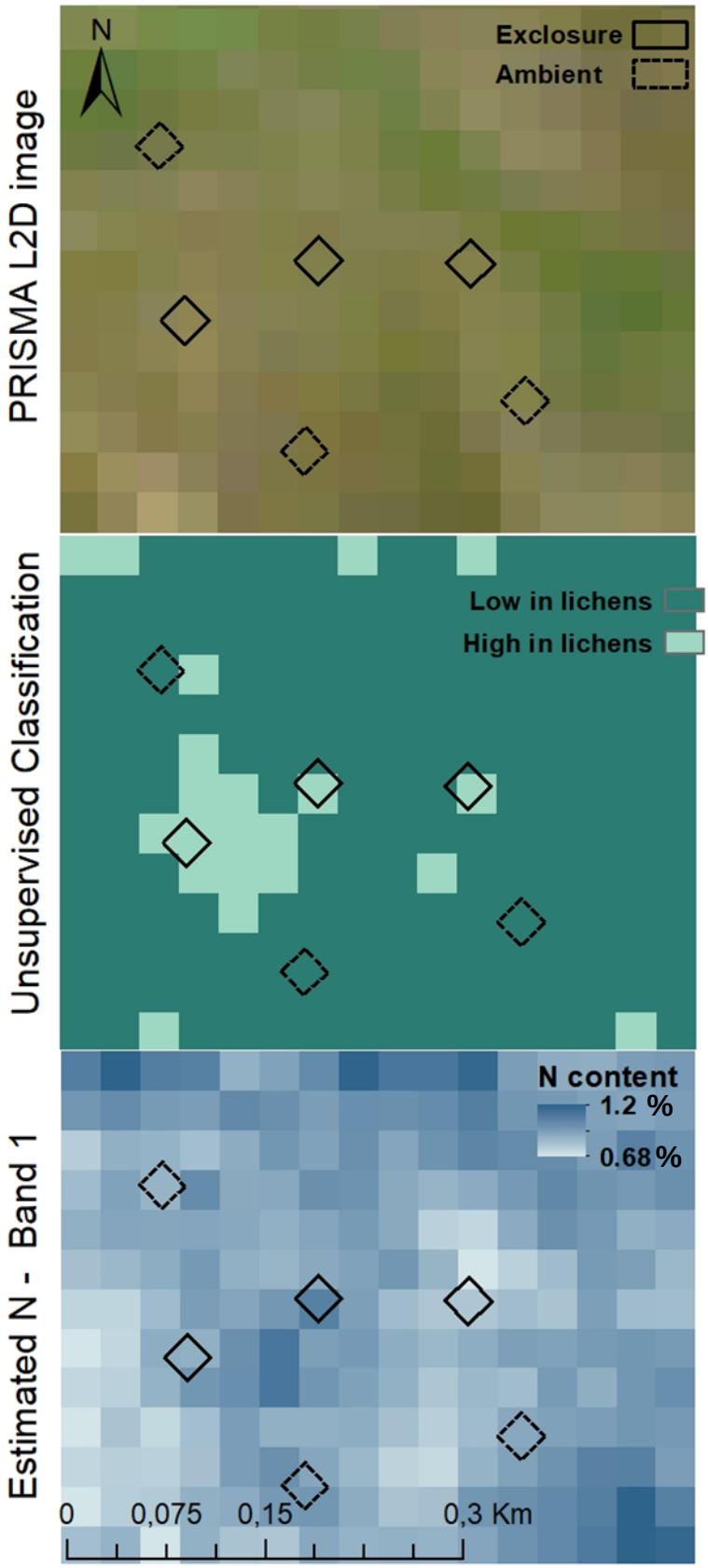

Figure 30. *The top figure shows the plots in Långfjället on a "True color" background, while the map in the middle displays the result from an unsupervised classification. The bottom map shows the regression functions from the MLR for band 1 applied over the unsupervised classification map from above. The estimated nitrogen values are based on the six plots' CWM of nitrogen (%).*

4. Discussion

4.1 Wavelengths Related to Nitrogen Content

4.1.1 Nitrogen Analysis

To answer the first research question of this project, the initial step was to determine the nitrogen content for the most abundant plant species in the plots of the study area. Through a standard IRMS analysis, the mean values for the % of nitrogen showed that, under both exclosure and ambient treatment, *Cladonia rangiferina* had the lowest N concentrations out of the four plant species studied (Table 5). This is consistent with literature, which states that most lichen species, including *Cladonia* species, are nitrogen poor (Olofsson et al., 2004; Staaland & Saeboe, 1993). Table 5 shows that nitrogen values for *Cladonia rangiferina* were only approximately 40 % of the concentrations measured for *E. hermaphroditum* or exclosures of *Calluna vulgaris* (30% comparing for ambient plots), and only 20 % compared to *B. nana*. The relationship between *Cladonia rangiferina* and *B. nana* for both exclosures and ambient plots are consistent with the result from Olofsson et al. (2004), where the lichen's nitrogen concentrations were approximately 20 % of new growth deciduous shrubs, for all grazing pressures. For the evergreen shrubs, the result from Olofsson et al. (2004) showed that nitrogen values of lichens were approximately 30 % of new growth evergreen shrubs (regardless of grazing pressure), while being 50 % of lightly grazed old biomass and 60 % for moderately to highly grazed old biomass (Olofsson et al., 2004). *B. nana* was the only deciduous plant investigated in this project, as *E. hermaphroditum* and *Calluna vulgaris* are both evergreen shrubs and lichens are an organism where algae and fungi live in symbiosis. Consequently, as there were not many species or samples collected caution should be taken when interpreting the results.

B. nana was the only vegetation grazed at the time of the field work. Reindeer are resourceful herbivores that shift their foraging preferences with the seasons (Tunón & Sjaggo, 2012). According to mountain reindeer herders, in the summer months, reindeer forage on green grasses, forbs, and leaves from *Betula* (birches) and *Salix* (willow) species (Inga & Danell, 2013). Shrubs like *Vaccinium* species and *E. hermaphroditum*, are part of the fall to spring diet according to mountain reindeer herders (Inga & Danell, 2013). Reindeer graze on lichens during winter conditions (Inga, 2007; Staaland & Saeboe, 1993; Tunón & Sjaggo, 2012), with a preference towards *Cladonia* species (Inga, 2007), and *Calluna vulgaris* (Warenberg, 1982, p. 26).

As mentioned previously, herbivores can impact the nitrogen cycling rate (Stark et al., 2023). Studies have shown that herbivores can both enhance (e.g., McNaughton, 1979; Olofsson et al., 2004) and inhibit (e.g., Pastor et al., 1993) this rate. For example, in Olofsson et al. (2004) reindeer were found to enhance nitrogen cycling, as indicated by the higher nitrogen values and lower microbial and soil C/N ratios observed in treatments with high grazing pressure. The main source behind the direction of the feedback from herbivores on the tundra ecosystems seems to be debatable. While studies have found that herbivores' effect on the nutrient cycling rate is dependent on the nutrient availability of the rangelands (Stark, 2007), this has also been challenged by studies showing that soil nutrient availability did not affect the grazing impact (e.g., Stark & Grellmann, 2002). It has also been suggested that it is the intensity of the grazing pressure, rather than then nutrient availability of the soil, which regulate the impact of herbivory

(Stark, 2007). The grazing history of the rangeland also seems to be a factor to consider when investigating herbivores effect on an ecosystem (Stark et al., 2023).

In this project all plant species except for *B. nana* had higher nitrogen concentrations and lower C/N ratios for exclosures than compared with ambient plots (Table 5), indicating that herbivores could possibly have an inhibiting effect on the rate of nitrogen cycling at out study site. As discussed above, *B. nana* was the only vegetation out of our four species that was grazed during the field work. Reindeer grazing appears to enhance the nitrogen uptake for *B. nana*, as the nitrogen values are higher and C/N ratios are lower for ambient plots (Table 5). Especially in more nutrient rich environments, increased allocation of nutrients to foliar biomass is one of the defense mechanisms that vegetation can use to compensate for herbivore grazing (Herms & Mattson, 1992). Plants can increase the supply of nitrogen to the foliage at the risk of defoliation by grazers, but with the benefit of increased photosynthetic potential (Díaz et al., 2016). For instance, Liu et al. (2017b) showed that the removal of two maize leaves enhanced nitrogen uptake to kernels while the removal of four to six leaves reduced nitrogen uptake. Since root samples were not collected, it is not possible to get a holistic view on nitrogen allocation in *B. nana*, i.e., how the higher nitrogen concentrations for above ground *B. nana* biomass in the ambient plots may have affected below ground nitrogen concentrations.

Two likely contributing factors to that herbivores appears to inhibit the rate of nitrogen cycling in Långfjället might be the intensity of grazing and the nutrient limited soil. Långfjället study site is near the lake Grövelsjön which lies within the year round grazing range (Lantbruksnämnden i Jämtlands län, 1990). Långfjället is a nutrient poor heath site as stated by Vowles et al. (2017b) who found results supporting that the site is transitioning from a graminoid-dominated state back into a shrub-dominated state, which is a change driven by factors other than grazing pressure (Vowles et al., 2017b). Shrubification in Långfjället has, during the period of 1995-2011, hindered the expansion of lichens in the exlosures and, together with grazing, has decreased lichen extent in the ambient plots (Vowles et al., 2017a; Vowles et al., 2017b). However, over both environmental treatments, the relative abundance of lichens showed a decrease while all evergreen shrubs show an increased over the time period (Vowles et al., 2017b). Both the decrease in lichens and increase in evergreen shrubs were slightly more pronounced in the ambient plots (Vowles et al., 2017b). During this period, the Idre new Sámi village had a cap of maximum 2 700 reindeer in its winter herd (Lantbruksnämnden i Jämtlands län, 1990). Despite this, the intensity of grazing pressure has, according to personal communications with a reindeer herder from Idre new Sámi village presented in Vowles et al. (2017b), increased during this period.

Standard parametric tests, such as Student's t-test, are recommended by Zeleny (2018) to avoid type 1 errors when working with CWMs under the hypothesis that there is a relationship between species attributes (nitrogen amount in the case of this study) and species composition. He suggests that to avoid type 1 errors, a standard parametric test should be performed using the null hypothesis that there are no statistically significant differences between sample attributes. The sample attributes in this study were the environmental treatments: exclosures vs ambient plots. The null hypothesis used in this project, for the Student's t-tests, was that for each species there was no statistical difference in measured nutrient concentrations between exclosures and ambient plots. Unexpectedly, only *E. hermaphroditum*, for N, ^{15}N, and C/N, and *Calluna vulgaris*, for ^{15}N, showed statistically significant p-values (Tables 6 & 7). The null hypothesis can be rejected for *E. hermaphroditum* and for ^{15}N values for *Calluna vulgaris*. The

statistical significances for the three remaining species (excluding ^{15}N for *Calluna vulgaris*) are insufficient to reject the null hypothesis. However, as each environmental condition only consisted of 3 plots respectively, it is possible that the sample size was too small to determine that a difference between the environmental conditions exists.

4.1.2 Remote Sensing Analysis

More than 95% of the variation from the PRISMA data could be explained by the first two principal component bands, PC 1, and PC 2 (Figure 22). In the correlation matrix (Figure 23), PC 1 correlates most to PRISMA bands 110 – 130 (~ 1510 – 1640 nm) but has a broad range of bands with high correlation in bands outside of these wavelengths. In contrast PC 2 seems to have high correlation only to the narrow wavelength bands around bands 2 – 4 (~ 410 – 430 nm). PC 2 and the "%IncMSE" (from the variable importance in the RF regression) results showed correlations to similar PRISMA bands, as the three highest values from the "%IncMSE" were bands 5, 2, and 4 (~ 410 – 430 nm). So, it appears that these bands are influential in the variation of the original PRISMA data and when trying to predict nitrogen content.

The results from the scatter plot of PC 1 vs PC 2 (Figure 21) did not show that the two different environmental traits formed two distinct clusters, as was expected. The dissimilarity seen for the fenced exclosures in Figure 21, could be due to the difference in the location of the PRISMA pixel vs the location of the exclosure plots as seen in Figure 12. The small sample size makes it difficult to discuss the scatter plot results much further beyond the cautious statement that there appears to be a dissimilarity in the exclosures.

During the data analysis, it became clear that the regression needed to be executed separately for exclosures and ambient plots. This was likely due to the higher lichen cover in the exclosures than in the ambient plots. The two linear regressions were then calculated for each wavelength band against the CWM of nitrogen in the MLR. Ideally, additional plant species would have been collected in field so that more of the heterogeneous vegetation could be accounted for in each of the respective environmental treatments.

The results from the MLR for PRISMA showed high R2 (over 0.7) values for all wavelength bands under band 35 (~680 nm), i.e., wavelength bands in the VIS. And all bands with an R2 >0.8 are under ~610 nm (band 28). MLR for Sentinel-2 bands, showed much lower R2 values than for the PRISMA bands (Table 10), and they were comparable to the lowest R2 values for the PRISMA wavelength bands in the NIR regions. The Sentinel-2 bands with the highest R2 values were B08 (for 10 m resolution) and B02 (for 20 m resolution). B08, which has a resolution of 10 m, overlaps with the B8A band and therefore the B08 band is not scaled up and included with the 20 m bands. The difference in R2 between B08 (10 m) at 0.36 and B8A (20 m) at 0.26 is likely due to the differences in spectral resolution between the two bands (Figure 1). The differences in R2 values between the PRISMA and the Sentinel-2 linear regressions could be attributed to the difference in spectral resolution, as the Sentinel-2 bands do not cover the full VIS, as the PRISMA sensor does. There is an additional Sentinel-2 wavelength band B01 which covers the blue region, however the spatial resolution for this band is 60 m.

PC 2 (from the PCA), "%IncMSE" (from the RF regression), and the result from the MLR, all showed high correlation to PRIMSA bands which are in the short wavelength end of the blue spectra. Bands 2-4 for PC 2, bands 2-5 for "IncMSE", and for the MLR all band from band 1-

23 had an R2 value of 0.9 or above. Thenkabail et al. (2013) used spectra from eight different crops to study optimal hyperspectral narrowbands and found a nitrogen absorption band at 405 nm. Rees et al. (2004) found that in the VIS, spectral signature curves for fruticose lichens (which *Cladonia rangiferina* belongs to), most of the fruticose lichens had a minimum at 405 nm, but minimums or slope changes varied in the range 410-470 nm. They put forward that this minimum feature in lichen's spectral curves, which they detected primarily over fruticose lichens, could be related to absorption of chlorophyll in the 430-450 nm range. Chlorophyll b has a larger peak at 460 nm and chlorophyll a has a weaker peak at 430 nm (Curran, 1989). Investigating the spectral curves for our study plots at 405 nm (band 1) in Figure 16, does show higher reflectance over the ambient plots and lower reflectance for exclosures. This is consistent with a weak minimum over exclosures which might then be lichen related. This is a deviation from the general trend in the spectral signature curves where ambient plots tend to show lower reflectance than the exclosures (Figure 15). Therefore, PRISMA band 1 was chosen as one of the bands in the unsupervised classification. The linear regression functions from band 1 were then also used to estimate nitrogen content over the whole area.

The result from the R function for variable importance using Random Forest ("VarSelRF"; Figure 25), showed high importance for bands 24-30, 33, and 36-38, which lies within the wavelengths 580 – 709 nm. This result could be related to the results from Mutanga et al. (2003) where they found highest correlation to chlorophyll content for the region 584 – 725 nm, and Carter (1993) who found that the wavelengths most sensitive to plant stress are at 535 – 640 nm and 685 – 700 nm. Bands 26 and 37, approximately 600 nm and 700 nm respectively, were chosen as two of the bands used to carry out the unsupervised classification.

"VarSelRF" (Figure 25), also showed that bands 43, 45, and 49-51 (760 – 840 nm), in the NIR spectrum, had high importance. Ollinger et al. (2008) found correlation between nitrogen and wavelengths in the 800-850 nm range, however, this has been challenged by Townsend et al. (2013) and Knyazikhin et al. (2013), who comment that the correlation observed was mainly due to canopy structure not nitrogen. From the MLR, the NIR range from around band 40 (~730 nm) to band 100 (~1330 nm) had the lowest R2 values and least explains the CWM of nitrogen. For this reason, it seems like these wavelength bands may be good at distinguishing between exclosures and ambient plots, but they do not appear to be related to CWM of nitrogen. Bands 45 and 51, approximately 780 nm and 840 nm respectively, were also used in the unsupervised classification. Bands 60, 108, 131, and 160 (approximately 940 nm, 1490 nm, 1730 nm, and 2140 nm) were also wavelength bands with high importance which were then used in the unsupervised classification. Out of these, bands 131 and 160 coincides with the nitrogen protein absorption features at 1730 nm and 2130 nm (Curran, 1989; Fourty et al., 1996).

The results from "VarSelRF" for Sentinel-2 was a bit different from PRIMSA, the bands with the most importance were B03 (~560 nm), and B05-B07 (~700-780 nm). The wavelength for B03 coincides with the shorter wavelength region that Carter (1993) detected at 535 – 640 nm, which he related to vegetation stress. Sentinel-2 bands B05-B07 lie within the red edge, and this region is commonly used in indexes which can give indications on vegetation health, character (e.g., NDVI), and state (Eismann, 2012).

Although the current study is based on a small sample size and despite its exploratory nature, this study contributes to and gives a suggested method for estimating nitrogen content. Given more field data, both over more plots and for more vegetation types, it would allow for a much

more robust nitrogen estimation over the site. It would also reduce the risk of overfitting as it would allow for more training and test data, while the additional plant species would better describe the heterogeneous vegetation in the plots.

4.2 PRISMA vs Sentinel-2

4.2.1 Visual Comparison of Spectral Curves

Perhaps the most interesting finding from the visual comparison graphs is that, for both PRISMA and Sentinel-2, the spectral signature curves for ambient plots tend to show lower reflectance than the exclosures (Figure 15). As the albedo for *Cladonia rangiferina* is high (Stoy et al., 2012), the difference in reflectance is likely to be related to the difference in lichen cover between the two environmental treatments. This is supported by Vowles et al. (2017a), where in their 3rd figure, one of the graphs describe how lichen cover in Långfjället, during the period of 1995 to 2011, has remained at constant levels in the exlosures while it has decreased in extent in the ambient plots. Inventory taken in 2022 (Brachmann, unpublished data of species occurrences), retrieved the averaged plot percent cover of *Cladonia rangiferina* and it shows similar results, which are as follows (in descending order of lichen cover): Plot 5 (exclosure), plot 1 (exclosure), plot 6 (ambient), plot 2 (ambient), plot 3 (exclosure), and plot 4 (ambient). The outlier in expected lichen cover is Plot 3 (exclosure), as it has a lower percent cover of lichens than Plot 6 and 2 (both ambient plots). It might be worth mentioning that the percent cover of a vegetation species is not synonymous with the total above ground biomass of said plant species. As previously stated in the method and materials section, in the field you could see a clear difference between the exclosures and the ambient plots, which is displayed in the two photographs in Figure 9.

Viewing the exclosures and ambient plot's spectral curves separately, we could try and evaluate whether the spectral signature curves are related to differences in lichen cover between the two environmental treatments. Examining only the exclosures (Figure 19), it appears that Plot 1 has higher reflectance than the other exclosures, for both satellite sensors. While, in the SWIR range Plot 3 shows the lowest reflectance for both satellites and in the NIR range for Sentinel-2, Plot 5 had the lowest reflectance. Looking further at only the ambient plots (Figure 20), it seems like Plot 4 has the lowest reflectance which is in accordance with the vegetation inventory in 2022. While Plot 6 had the highest reflectance in the SWIR range for the PRISMA spectral curves. In contrast, Plot 2 had the highest reflectance for Sentinel-2 in the NIR range. From these comparisons, the SWIR region appears to correlate well with the 2022 lichen cover inventory, with the exception that Plot 1 showed higher reflectance than plot 5. The VIS regions, with the same exception, also seems to agree with the lichen cover. However, this region is a little harder to interpret as the spectral curves are more indistinguishable from each other. The NIR region seems to deviate more from the order of the spectral curves seen in the adjacent sections. The NIR region is a section which is most influenced by scatter caused by the internal structure in leaves rather than foliar components, which are the main drivers of absorption features in the other two sections (Eismann, 2012).

These two spectral images were acquired one day apart, towards the end of July 2021 and during the same time of day. The largest differences observed between PRISMA and Sentinel-2 spectral data occur in the VIS part of the spectrum prior to the red edge (Figure 15), although a clear difference can also be observed over the NIR spectrum. However, while the Sentinel-2

spectral data have higher reflectance than the PRISMA data in the VIS range, the dynamic is the opposite in the NIR range. The observed difference between measured reflectance of PRISMA against Sentinel-2 is likely due to varying sensor characteristics. It may also be due to different atmospheric correction regimes or with the sensitivity of each sensor. These conjectures are supported by Niroumand-Jadidi et al. (2020) who compared PRISMA level 2D image with Sentinel-2 data, applied for water quality sensing, and reported that PRISMA had lower detected reflectance than Sentinel-2. They also postulated that the difference may be attributable to different atmospheric corrections. Another possibility they put forth was the difference in temporal resolution (also a one-day gap) which they suggest could account for a small part of the difference.

Sentinel-2 bands B02, B03, and B04, display a clear difference between exclosures and ambient plots that is not mirrored with the PRISMA bands, which are more intertwined. The same clear division, between exclosures and ambient plots, can be seen for both Sentinel-2 and PRISMA in NIR region (Figure 17). For instance, in Figure 17 Sentinel-2 shows a dip in reflectance of for band B08 in ambient plots but not for exclosures. B08 is, compared with the other Sentinel-2 bands in the NIR region, the broadest wavelength band (Figure 1). For the SWIR range, no noticeable difference between exclosures and ambient plots can be observed for either satellite (Figure 18). That the PRIMSA spectral curves interweave more than the Sentinel-2 data, could potentially be attributed to the differences in spatial and spectral resolution. PRISMA has a higher spectral resolution, while Sentinel-2 has a lower spatial resolution. The difference cannot be attributed to radiometric quantization, as the two sensors have the same radiometric resolution of 12 bit (Table 1 & 2). Additionally, the higher spatial resolution would make the PRISMA dataset more susceptible to the mixed pixel problem (Boyd & Foody, 2011). The problem would, in the case of this report, be that the PRIMSA pixel size would be too large to represent the reflectance of the plot's environmental treatments (Boyd & Foody, 2011). It seems more likely the mixed signals in PRISMA to be caused by the pixel location in relation to the plot location (Figure 12), as the PRISMA pixel with most area within the respective plots was selected to represent that plot.

5. Conclusion

In this project, the aim was to investigate if hyperspectral satellite data could be used to differentiate between grazed and ungrazed tundra, as well as estimate nitrogen content of the vegetation over this landscape. The first research question of this project was to determine which hyperspectral wavelength bands would be best suited for determining nitrogen content from vegetation measured over a tundra reindeer grazing site. The result from the MLR supports using chlorophyll as a proxy for nitrogen content. For the MLR, the PRISMA wavelength bands below ~680 nm (band 35) all had R2 values >0.7, while all bands with an R2 >0.8 were under ~610 nm (band 28). In particular, this study identified that band 1, at 405 nm, was best suited for determining nitrogen content in grazed and ungrazed tundra landscapes. This was due to the wavelength at 405 nm having a connection to a minimum in lichen spectral curves (Rees et al., 2004) and to an absorption for nitrogen (Thenkabail et al., 2013). PRISMA's band 1 was therefore chosen to estimate nitrogen content over the study area, using separate regression equations for exclosures vs ambient plots.

The second research question was to investigate if the PRISMA hyperspectral sensor can more accurately differentiate between grazed and ungrazed tundra vegetation than the Sentinel-2 multispectral sensor. The high spectral resolution of PRISMA is needed to identify narrow absorption features. However, when it comes to only differentiating between grazed and ungrazed rangeland both PRIMSA and Sentinel-2 have their benefits and drawbacks. As mentioned PRISMA has a higher spectral resolution, while Sentinel-2 has a lower spatial resolution.

One source of uncertainty is that from the IRMS results one ambient plot (Plot 6) had concentrations which looked incorrect. The decision was made to exclude these values. Since the sample size was so small, removing these values makes it even more important to take caution into account when interpreting the results. Another source of uncertainty is that the PRISMA data did not have accurate geographic coordinate registration, and the image was noticeably displaced when compared to Sentinel-2 and orthophotos. The manual realignment was necessary but should be kept in mind as a potential weakness. Additionally, the geographical positioning system used in the field work was from a phone so the accuracy of the position of the plots (at least $\pm$3m) was not optimal.

Although the results should be interpreted with caution, due to the small sample size of the reference data, it shows potential possibilities of what could be done with biochemical trait estimation via remote sensing. This study contributes to the wider scientific field by giving a suggested method for estimating nitrogen content and by giving a suggestion for which hyperspectral wavelength band is best suited for determining nitrogen content in a tundra landscape. Future projects may want to collect more sample data, both more samples and for more plant species. Since PRISMA is a relatively new sensor, few studies have been published regarding its application. In this decade, several new hyperspectral satellites will be launched, and applications will likely increase. Hyperspectral satellites expected to launch towards the end of the decade are for instance ESA's Sentinel-10 CHIME and NASA's the Surface Biology and Geology (ESA, 2021).

6. References

ASI. (2020). *PRISMA Products Specification Document Issue 2.3*. Retrieved 2023-04-14 from http://prisma.asi.it/missionselect/docs/PRISMA%20Product%20Specifications_Is2_3.pdf

Beck, H. E., Zimmermann, N. E., McVicar, T. R., Vergopolan, N., Berg, A., & Wood, E. F. (2018). Present and future Köppen-Geiger climate classification maps at 1-km resolution. *Scientific Data*, *5*(1), 180214. https://doi.org/10.1038/sdata.2018.214

Belgiu, M., & Drăguţ, L. (2016). Random forest in remote sensing: A review of applications and future directions. *ISPRS journal of photogrammetry and remote sensing*, *114*, 24-31. https://doi.org/10.1016/j.isprsjprs.2016.01.011

Berger, K., Verrelst, J., Féret, J.-B., Hank, T., Wocher, M., Mauser, W., & Camps-Valls, G. (2020a). Retrieval of aboveground crop nitrogen content with a hybrid machine learning method. *International Journal of Applied Earth Observation and Geoinformation*, *92*, 102174. https://doi.org/https://doi.org/10.1016/j.jag.2020.102174

Bernes, C., Bråthen, K. A., Forbes, B. C., Speed, J. D., & Moen, J. (2015). What are the impacts of reindeer/caribou (Rangifer tarandus L.) on arctic and alpine vegetation? A systematic review. *Environmental Evidence*, *4*(1). https://doi.org/10.1186/s13750-014-0030-3

Boyd, D. S., & Foody, G. M. (2011). An overview of recent remote sensing and GIS based research in ecological informatics. *Ecological informatics*, *6*(1), 25-36. https://doi.org/10.1016/j.ecoinf.2010.07.007

Campbell, J. B., Wynne, R. H., & Thomas, V. A. (2022). *Introduction to Remote Sensing*. Guilford Publications. http://ebookcentral.proquest.com/lib/gu/detail.action?docID=7012355

Carter, G. A. (1993). Responses of Leaf Spectral Reflectance to Plant Stress. *American journal of botany*, *80*(3), 239. https://doi.org/10.2307/2445346

Cavender-Bares, J., Gamon, J. A., & Townsend, P. A. (2020). How the Optical Properties of Leaves Modify the Absorption and Scattering of Energy and Enhance Leaf Functionality. In (pp. 349-384). Switzerland: Springer International Publishing AG. https://doi.org/10.1007/978-3-030-33157-3_14

Copernicus. (2018). *Sentinel-2*. European Commission. Retrieved 2023-04-15 from https://www.copernicus.eu/sites/default/files/2018-10/Copernicus_Sentinel-2_Factsheet_13042018.pdf

Cronin, M. A., Patton, J. C., Balmysheva, N., & MacNeil, M. D. (2003). Genetic variation in caribou and reindeer (Rangifer tarandus) [https://doi.org/10.1046/j.1365-2052.2003.00927.x]. *Animal Genetics*, *34*(1), 33-41. https://doi.org/https://doi.org/10.1046/j.1365-2052.2003.00927.x

Curran, P. J. (1989). Remote sensing of foliar chemistry. *Remote Sensing of Environment*, *30*(3), 271-278. https://doi.org/https://doi.org/10.1016/0034-4257(89)90069-2

Diaz-Uriarte, R. (2007). GeneSrF and varSelRF: a web-based tool and R package for gene selection and classification using random forest. *BMC bioinformatics*, *8*(1), 328-328. https://doi.org/10.1186/1471-2105-8-328

Díaz, S., Kattge, J., Cornelissen, J. H. C., Wright, I. J., Lavorel, S., Dray, S., Reu, B., Kleyer, M., Wirth, C., Colin Prentice, I., Garnier, E., Bönisch, G., Westoby, M., Poorter, H., Reich, P. B., Moles, A. T., Dickie, J., Gillison, A. N., Zanne, A. E., . . . Gorné, L. D. (2016). The global spectrum of plant form and function. *Nature*, *529*(7585), 167-171. https://doi.org/10.1038/nature16489

Drusch, M., Del Bello, U., Carlier, S., Colin, O., Fernandez, V., Gascon, F., Hoersch, B., Isola, C., Laberinti, P., Martimort, P., Meygret, A., Spoto, F., Sy, O., Marchese, F., & Bargellini, P. (2012). Sentinel-2: ESA's Optical High-Resolution Mission for GMES Operational Services. *Remote Sensing of Environment*, *120*, 25-36. https://doi.org/https://doi.org/10.1016/j.rse.2011.11.026

Eismann, M. T. (2012). *Hyperspectral Remote Sensing* (Vol. v.PM210). Berlin: SPIE. https://doi.org/10.1117/3.899758

Eriksson, O., Niva, M., & Caruso, A. (2007). Use and abuse of reindeer range. *Acta Phytogeographica Suecica*, *87*, 1–101.

ESA. (2015). *Sentinel-2 User Handbook*. Retrieved 2023-04-16 from https://sentinels.copernicus.eu/documents/247904/685211/Sentinel-2_User_Handbook.pdf/8869acdf-fd84-43ec-ae8c-3e80a436a16c?t=1438278087000

ESA. (2021). *Going hyperspectral for CHIME*. Retrieved 2023-05-29 from https://www.esa.int/Applications/Observing_the_Earth/Copernicus/Going_hyperspectral_for_CHIME

Fourty, T., Baret, F., Jacquemoud, S., Schmuck, G., & Verdebout, J. (1996). Leaf optical properties with explicit description of its biochemical composition: Direct and inverse problems [Article]. *Remote Sensing of Environment*, *56*(2), 104-117. https://doi.org/10.1016/0034-4257(95)00234-0

Freeman, E. A., Moisen, G. G., Coulston, J. W., & Wilson, B. T. (2016). Random forests and stochastic gradient boosting for predicting tree canopy cover: Comparing tuning processes and model performance. *Canadian journal of forest research*, *46*(3), 323-339. https://doi.org/10.1139/cjfr-2014-0562

Furberg, M., Evengård, B., & Nilsson, M. (2011). Facing the limit of resilience: perceptions of climate change among reindeer herding Sami in Sweden. *Global Health Action*, *4*(1), 8417. https://doi.org/10.3402/gha.v4i0.8417

Ghosh, A., Fassnacht, F. E., Joshi, P. K., & Koch, B. (2014). A framework for mapping tree species combining hyperspectral and LiDAR data: Role of selected classifiers and sensor across three spatial scales. *International Journal of Applied Earth Observation and Geoinformation*, *26*(1), 49-63. https://doi.org/10.1016/j.jag.2013.05.017

Green, A. A., Berman, M., Switzer, P., & Craig, M. D. (1988). A transformation for ordering multispectral data in terms of image quality with implications for noise removal. *IEEE transactions on geoscience and remote sensing*, *26*(1), 65-74. https://doi.org/10.1109/36.3001

Herms, D. A., & Mattson, W. J. (1992). The Dilemma of Plants: To Grow or Defend. *The Quarterly Review of Biology*, *67*(3), 283-335. http://www.jstor.org.ezproxy.ub.gu.se/stable/2830650

Hexagon Geospatial. (2022). *ERDAS IMAGINE Online Help* http://localhost:8080/imaginehelp/html/#/home/overview_of_imagine/10/11

Holand, Ø., Mizin, I., & Weladji, R. B. (2022). Reindeer Rangifer tarandus (Linnaeus, 1758). In (pp. 247-276). Springer International Publishing. https://doi.org/10.1007/978-3-030-24475-0_24

Inga, B. (2007). Reindeer (*Rangifer tarandus tarandus*) feeding on lichens and mushrooms; traditional ecological knowledge among reindeer-herding Sámi in northern Sweden. *Rangifer*, *27*(2), 93-106. https://doi.org/https://doi.org/10.7557/2.27.2.163

Inga, B., & Danell, Ö. (2013). Traditional ecological knowledge among Sami reindeer herders in northern Sweden about vascular plants grazed by reindeer. *Rangifer*, *32*(1), 1-17. https://doi.org/10.7557/2.32.1.2233

Knyazikhin, Y., Schull, M. A., Stenberg, P., Mõttus, M., Rautiainen, M., Yang, Y., Marshak, A., Carmona, P. L., Kaufmann, R. K., Lewis, P., Disney, M. I., Vanderbilt, V., Davis, A. B., Baret, F., Jacquemoud, S., Lyapustin, A., & Myneni, R. B. (2013). Hyperspectral remote sensing of foliar nitrogen content. *Proceedings of the National Academy of Sciences - PNAS*, *110*(3), 811-812. https://doi.org/10.1073/pnas.1210196109

Kokaly, R. F. (2001). Investigating a Physical Basis for Spectroscopic Estimates of Leaf Nitrogen Concentration. *Remote Sensing of Environment*, *75*(2), 153-161. https://doi.org/10.1016/S0034-4257(00)00163-2

Kokaly, R. F., Asner, G. P., Ollinger, S. V., Martin, M. E., & Wessman, C. A. (2009). Characterizing canopy biochemistry from imaging spectroscopy and its application to ecosystem studies. *Remote Sensing of Environment*, *113*, S78-S91. https://doi.org/10.1016/j.rse.2008.10.018

Kramer, H. J. (2003, 2022). *History*. Retrieved 2023-05-14 from https://www.eoportal.org/observing-the-earth

Lantbruksnämnden i Jämtlands län. (1990). *Utvecklingsplanering; Markanvändningsredovisning och driftplanering för Idre nya sameby*. Retrieved from https://www.samediggi.se/9374

Lantmäteriet. (n.d.). *Geodata Extraction Tool* Retrieved 2022-11-11 from https://zeus.slu.se/get/?drop=

Lee, J. B., Woodyatt, A. S., & Berman, M. (1990). Enhancement of high spectral resolution remote-sensing data by a noise-adjusted principal components transform. *IEEE transactions on geoscience and remote sensing*, *28*(3), 295-304. https://doi.org/10.1109/36.54356

Liu, N., Budkewitsch, P., & Treitz, P. (2017a). Examining spectral reflectance features related to Arctic percent vegetation cover: Implications for hyperspectral remote sensing of Arctic tundra. *Remote Sensing of Environment*, *192*, 58-72. https://doi.org/10.1016/j.rse.2017.02.002

Liu, T., Huang, R., Cai, T., Han, Q., & Dong, S. (2017b). Optimum Leaf Removal Increases Nitrogen Accumulation in Kernels of Maize Grown at High Density. *Scientific Reports*, *7*(1), 39601. https://doi.org/10.1038/srep39601

Loizzo, R., Daraio, M., Guarini, R., Longo, F., Lorusso, R., Dini, L., & Lopinto, E. (2019, 28 July-2 Aug. 2019). Prisma Mission Status and Perspective. IGARSS 2019 - 2019 IEEE International Geoscience and Remote Sensing Symposium,

Loizzo, R., Guarini, R., Longo, F., Scopa, T., Formaro, R., Facchinetti, C., & Varacalli, G. (2018, 22-27 July 2018). Prisma: The Italian Hyperspectral Mission. IGARSS 2018 - 2018 IEEE International Geoscience and Remote Sensing Symposium,

McNaughton, S. J. (1979). Grazing as an optimization process: grass-ungulate relationships in the Serengeti [National Park, Tanzania]. *The American naturalist*, *113*(5), 691-703. https://doi.org/10.1086/283426

Meredith, M., Sommerkorn, M., Cassotta, S., Derksen, C., Ekaykin, A., Hollowed, A., Kofinas, G., Mackintosh, A., Melbourne-Thomas, J., Muelbert, M. M. C., Ottersen, G., Pritchard, H., & Schuur, E. A. G. (2019). Polar Regions. In *IPCC Special Report on the Ocean and Cryosphere in a Changing Climate*.

Montesinos López, O. A., Montesinos López, A., & Crossa, J. (2022). Overfitting, Model Tuning, and Evaluation of Prediction Performance. In O. A. Montesinos López, A. Montesinos López, & J. Crossa (Eds.), *Multivariate Statistical Machine Learning Methods for Genomic Prediction* (pp. 109-139). Springer International Publishing. https://doi.org/10.1007/978-3-030-89010-0_4

Mutanga, O., Skidmore, A. K., & van Wieren, S. (2003). Discriminating tropical grass (Cenchrus ciliaris) canopies grown under different nitrogen treatments using spectroradiometry. *ISPRS journal of photogrammetry and remote sensing*, *57*(4), 263-272. https://doi.org/10.1016/S0924-2716(02)00158-2

Niroumand-Jadidi, M., Bovolo, F., & Bruzzone, L. (2020). Water quality retrieval from PRISMA hyperspectral images: First experience in a turbid lake and comparison with sentinel-2. *Remote sensing (Basel, Switzerland)*, *12*(23), 1-21. https://doi.org/10.3390/rs12233984

Ollinger, S. V., Richardson, A. D., Martin, M. E., Hollinger, D. Y., Frolking, S. E., Reich, P. B., Plourde, L. C., Katul, G. G., Munger, J. W., Oren, R., Smith, M. L., Paw U, K. T., Bolstad, P. V., Cook, B. D., Day, M. C., Martin, T. A., Monson, R. K., & Schmid, H. P. (2008). Canopy nitrogen, carbon assimilation, and albedo in temperate and boreal forests: Functional relations and potential climate feedbacks. *Proceedings of the National Academy of Sciences*, *105*(49), 19336-19341. https://doi.org/10.1073/pnas.0810021105

Olofsson, J., Stark, S., & Oksanen, L. (2004). Reindeer influence on ecosystem processes in the tundra. *Oikos*, *105*(2), 386-396. https://doi.org/10.1111/j.0030-1299.2004.13048.x

Pape, R., & Löffler, J. (2012). Climate Change, Land Use Conflicts, Predation and Ecological Degradation as Challenges for Reindeer Husbandry in Northern Europe: What do We Really Know After Half a Century of Research? *Ambio*, *41*(5), 421-434. https://doi.org/10.1007/s13280-012-0257-6

Pastor, J., Dewey, B., Naiman, R. J., McInnes, P. F., & Cohen, Y. (1993). Moose browsing and soil fertility in the boreal forests of Isle Royale National Park. *Ecology (Durham)*, *74*(2), 467-480. https://doi.org/10.2307/1939308

Rafstedt, T. (1982). Vegetationskarta över de svenska fjällen (Vegetation map of the Swedish mountains). In. Stockholm: Naturvårdsverket.

Rantanen, M., Karpechko, A. Y., Lipponen, A., Nordling, K., Hyvärinen, O., Ruosteenoja, K., Vihma, T., & Laaksonen, A. (2022). The Arctic has warmed nearly four times faster than the globe since 1979. *Communications Earth & Environment*, *3*(1), 168. https://doi.org/10.1038/s43247-022-00498-3

Rees, W. G., Tutubalina, O. V., & Golubeva, E. I. (2004). Reflectance spectra of subarctic lichens between 400 and 2400 nm. *Remote Sensing of Environment*, *90*(3), 281-292. https://doi.org/https://doi.org/10.1016/j.rse.2003.12.009

Reich, P. B., & Oleksyn, J. (2004). Global patterns of plant leaf N and P in relation to temperature and latitude. *Proceedings of the National Academy of Sciences*, *101*(30), 11001-11006. https://doi.org/doi:10.1073/pnas.0403588101

Samefolkets Egen Tidning. (1925). Landshövding Kvarnzelius ingriper till förmån för sameh i Idre. Renstängslen fylla sin uppgift. In *Samefolkets Egen Tidning (S.E.T.)* (Vol. 3, pp. 21-22). Trotsgatan 63, Falun.

Samefolkets Egen Tidning. (1926). Skall vårt lands värdefullaste renbeteslands spolieras. In *Samefolkets Egen Tidning (S.E.T.)* (Vol. 1, pp. 2-4). Trotsgatan 63, Falun.

Sametinget. (2016). *Samebyarnas betesområden* Planeringskatalogen. https://ext-geodatakatalog-forv.lansstyrelsen.se/PlaneringsKatalogen/GetMetaDataById?id=a216dea8-bfcb-4984-a18b-3a421cde2d57_C#allMetadataTab

Schott, J. R. (2007). *Remote sensing: the image chain approach*. New York: Oxford University Press.

Sercon. (2018). HS20-22 User's Manual V2.0. Retrieved 2023-06-25, from https://sercongroup.com/wp-content/uploads/2018/03/HS20-22-Manual-V2.0.pdf

SMHI. (n.d.). *Ladda ner meteorologiska observationer*. Retrieved 2022-10-20 from https://www.smhi.se/data/meteorologi/ladda-ner-meteorologiska-observationer#param=airtemperatureInstant,stations=core

Soininen, E. M., Barrio, I. C., Bjørkås, R., Björnsdóttir, K., Ehrich, D., Hopping, K., Kaarlejärvi, E., Kolstad, A. L., Abdulmanova, S., Björk, R. G., Bueno, C. G., Eischeid, I., Higgens, R. F., Forbey, J. S., Gignac, C., Gilg, O., Den Herder, M., Holm, H. S., Hwang, B. C., . . . Speed, J. D. M. (2021). Location of studies and evidence of effects of herbivory on Arctic vegetation: a systematic map. *Environmental Evidence*, *10*(1). https://doi.org/10.1186/s13750-021-00240-0

Staaland, H., & Saeboe, S. (1993). Forage diversity and nutrient supply of reindeer. *Rangifer*, *13*(3).

Stark, S. (2007). Nutrient Cycling in the Tundra. In P. Marschner & Z. Rengel (Eds.), *Nutrient Cycling in Terrestrial Ecosystems* (pp. 309-331). Springer Berlin Heidelberg. https://doi.org/10.1007/978-3-540-68027-7_11

Stark, S., & Grellmann, D. (2002). Soil Microbial Responses to Herbivory in an Arctic Tundra Heath at Two Levels of Nutrient Availability. *Ecology (Durham)*, *83*(10), 2736-2744. https://doi.org/https://doi.org/10.1890/0012-9658(2002)083[2736:SMRTHI]2.0.CO;2

Stark, S., Horstkotte, T., Kumpula, J., Olofsson, J., Tømmervik, H., & Turunen, M. (2023). The ecosystem effects of reindeer (Rangifer tarandus) in northern Fennoscandia: Past, present and future. *Perspectives in plant ecology, evolution and systematics*, *58*, 125716. https://doi.org/10.1016/j.ppees.2022.125716

Stein, L. Y., & Klotz, M. G. (2016). The nitrogen cycle. *Current biology*, *26*(3), R94-R98. https://doi.org/10.1016/j.cub.2015.12.021

Stoy, P. C., Street, L. E., Johnson, A. V., Prieto-Blanco, A., & Ewing, S. A. (2012). Temperature, Heat Flux, and Reflectance of Common Subarctic Mosses and Lichens under Field Conditions: Might Changes to Community Composition Impact Climate-Relevant Surface Fluxes? *Arctic, antarctic, and alpine research*, *44*(4), 500-508. https://doi.org/10.1657/1938-4246-44.4.500

Thenkabail, P. S., Mariotto, I., Gumma, M. K., Middleton, E. M., Landis, D. R., & Huemmrich, K. F. (2013). Selection of Hyperspectral Narrowbands (HNBs) and Composition of Hyperspectral Twoband Vegetation Indices (HVIs) for Biophysical Characterization and Discrimination of Crop Types Using Field Reflectance and Hyperion/EO-1 Data. *IEEE journal of selected topics in applied earth observations and remote sensing*, *6*(2), 427-439. https://doi.org/10.1109/JSTARS.2013.2252601

Townsend, P. A., Serbin, S. P., Kruger, E. L., & Gamon, J. A. (2013). Disentangling the contribution of biological and physical properties of leaves and canopies in imaging spectroscopy data. *Proceedings of the National Academy of Sciences - PNAS*, *110*(12), E1074-E1074. https://doi.org/10.1073/pnas.1300952110

Tunón, H., & Sjaggo, B. S. (Eds.). (2012). *Ájddo – reflektioner kring biologisk mångfald i renarnas spår*. CBM:s skriftserie nr 68. Sametinget, Kiruna & Centrum för biologisk mångfald,

Uppsala. https://www.slu.se/globalassets/ew/org/centrb/cbm/dokument/publikationer-cbm/cbm-skriftserie/cbmskrift68ajddo.pdf.
Van Cleemput, E., Vanierschot, L., Fernández-Castilla, B., Honnay, O., & Somers, B. (2018). The functional characterization of grass- and shrubland ecosystems using hyperspectral remote sensing: trends, accuracy and moderating variables. *Remote Sensing of Environment*, *209*, 747-763. https://doi.org/10.1016/j.rse.2018.02.030
Vangi, E., D'amico, G., Francini, S., Giannetti, F., Lasserre, B., Marchetti, M., & Chirici, G. (2021). The new hyperspectral satellite prisma: Imagery for forest types discrimination. *Sensors (Basel, Switzerland)*, *21*(4), 1-19. https://doi.org/10.3390/s21041182
Vors, L. S., & Boyce, M. S. (2009). Global declines of caribou and reindeer: CARIBOU REINDEER DECLINE. *Global change biology*, *15*(11), 2626-2633. https://doi.org/10.1111/j.1365-2486.2009.01974.x
Vowles, T., Gunnarsson, B., Molau, U., Hickler, T., Klemedtsson, L., & Björk, R. G. (2017a). Expansion of deciduous tall shrubs but not evergreen dwarf shrubs inhibited by reindeer in Scandes mountain range. *Journal of Ecology*, *105*(6), 1547-1561. https://doi.org/10.1111/1365-2745.12753
Vowles, T., Lovehav, C., Molau, U., & Björk, R. G. (2017b). Contrasting impacts of reindeer grazing in two tundra grasslands. *Environmental Research Letters*, *12*(3), 034018. https://doi.org/10.1088/1748-9326/aa62af
Warenberg, K. (1982). *Reindeer forage plants in the early grazing season : growth and nutritional content in relation to climatic conditions* Diss. Uppsala : Univ.].
Zeleny, D. (2018). Which results of the standard test for community-weighted mean approach are too optimistic? *Journal of vegetation science*, *29*(6), 953-966. https://doi.org/10.1111/jvs.12688

Appendix

Appendix 1

Table 1. *The first column shows the central wavelength for each respective PRISMA band (column two). "Bad" band name refers to the bands remaining after unwanted PRIMSA bands were removed.*

Central Wavelengths [nm]	PRISMA band name	"Bad" band name
402,4	1	1
411,3	2	2
419,4	3	3
427,0	4	4
434,3	5	5
441,7	6	6
449,0	7	7
456,4	8	8
463,7	9	9
470,9	10	10
478,2	11	11
485,4	12	12
492,7	13	13
500,1	14	14
507,7	15	15
515,2	16	16
522,9	17	17
530,7	18	18
538,5	19	19
546,5	20	20
554,6	21	21
562,7	22	22
571,0	23	23
579,4	24	24
587,8	25	25
596,5	26	26
605,4	27	27
614,2	28	28
623,2	29	29

632,1	30	30
641,3	31	31
650,8	32	32
660,3	33	33
669,8	34	34
679,5	35	35
689,4	36	36
699,1	37	37
709,0	38	38
719,2	39	39
729,2	40	40
739,4	41	41
749,7	42	42
760,1	43	43
770,5	44	44
780,9	45	45
791,4	46	46
801,9	47	47
812,5	48	48
823,1	49	49
833,8	50	50
844,4	51	51
855,2	52	52
865,9	53	53
876,6	54	54
887,3	55	55
898,0	56	-
908,6	57	56
919,2	58	57
929,4	59	58
939,9	60	59
943,0	61	60
951,0	62	61
951,4	63	62
959,5	64	63
962,3	65	64
969,4	66	65
972,6	67	66
978,7	68	67

988,4	69	68
998,4	70	69
1008,2	71	70
1018,0	72	71
1028,8	73	72
1037,8	74	73
1047,4	75	74
1057,4	76	75
1067,6	77	76
1078,0	78	77
1088,6	79	78
1099,1	80	79
1109,7	81	80
1120,5	82	81
1131,1	83	82
1141,9	84	83
1152,5	85	84
1163,5	86	85
1174,5	87	86
1185,4	88	87
1196,2	89	88
1207,1	90	89
1217,7	91	90
1229,0	92	91
1240,1	93	92
1250,8	94	93
1262,3	95	94
1273,3	96	95
1284,3	97	96
1295,2	98	97
1306,0	99	98
1317,0	100	99
1328,1	101	100
1338,9	102	101
1349,6	103	-
1360,8	104	-
1372,7	105	-
1383,0	106	-
1394,5	107	-

1405,4	108	-
1416,3	109	-
1427,1	110	102
1438,2	111	103
1448,9	112	104
1459,1	113	105
1469,7	114	106
1480,6	115	107
1491,2	116	108
1501,8	117	109
1512,4	118	110
1523,0	119	111
1533,6	120	112
1544,0	121	113
1554,6	122	114
1565,1	123	115
1575,4	124	116
1585,6	125	117
1596,0	126	118
1606,2	127	119
1616,6	128	120
1626,8	129	121
1636,9	130	122
1647,0	131	123
1656,8	132	124
1667,0	133	125
1677,1	134	126
1687,2	135	127
1697,0	136	128
1706,8	137	129
1716,6	138	130
1726,4	139	131
1736,3	140	132
1745,9	141	133
1755,5	142	134
1765,3	143	135
1774,9	144	136
1784,4	145	137
1793,7	146	138

1803,4	147	-
1812,8	148	-
1822,1	149	-
1831,7	150	-
1841,0	151	-
1850,3	152	-
1859,3	153	-
1868,0	154	-
1878,5	155	-
1886,8	156	-
1895,8	157	-
1904,6	158	-
1914,0	159	-
1923,1	160	-
1932,0	161	-
1940,8	162	-
1949,6	163	-
1958,4	164	-
1967,1	165	139
1975,8	166	140
1984,5	167	141
1993,3	168	142
2001,8	169	143
2010,4	170	144
2019,0	171	145
2027,5	172	146
2036,0	173	147
2044,4	174	148
2052,8	175	149
2061,1	176	150
2069,5	177	151
2077,8	178	152
2086,1	179	153
2094,4	180	154
2102,5	181	155
2110,8	182	156
2119,0	183	157
2127,1	184	158
2135,2	185	159

2143,2	186	160
2151,1	187	161
2159,3	188	162
2167,3	189	163
2175,1	190	164
2183,2	191	165
2190,8	192	166
2198,9	193	167
2206,6	194	168
2214,3	195	169
2222,2	196	170
2229,8	197	171
2237,6	198	172
2245,2	199	173
2252,8	200	174
2260,6	201	175
2268,0	202	176
2275,8	203	177
2283,3	204	178
2290,6	205	179
2298,3	206	180
2305,5	207	181
2312,9	208	182
2320,6	209	183
2327,6	210	184
2335,2	211	185
2342,6	212	186
2349,6	213	187
2357,0	214	188
2364,4	215	189
2371,3	216	190
2378,5	217	191
2385,8	218	192
2392,8	219	193
2399,8	220	194
2407,3	221	195
2414,2	222	196
2421,0	223	197
2428,4	224	198

2435,3	225	199
2442,2	226	200
2448,9	227	-
2456,3	228	-
2462,8	229	-
2469,4	230	-
2476,8	231	-
2483,6	232	-
2490,0	233	-
2496,9	234	-

Appendix 2

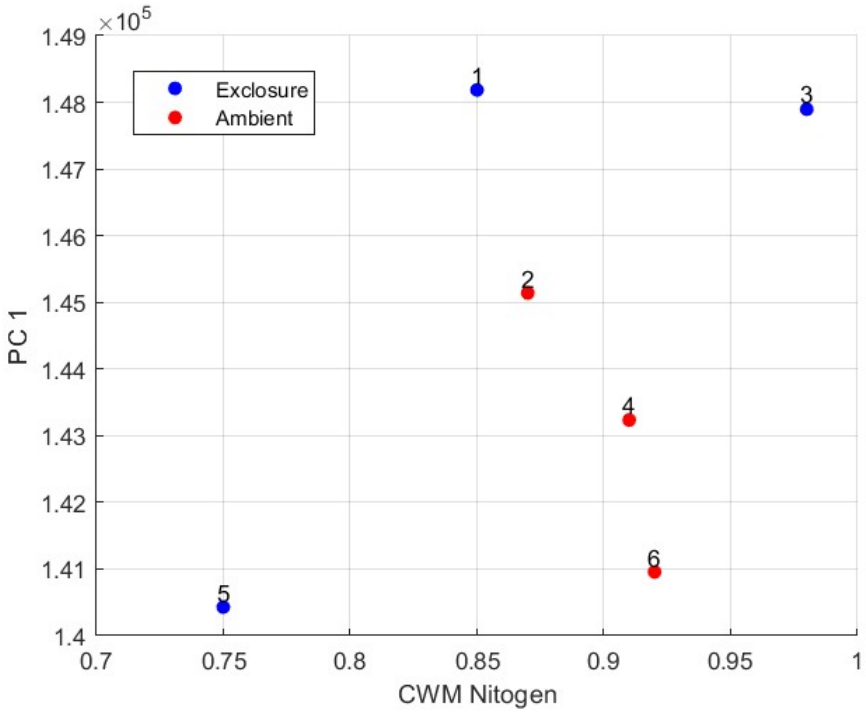

Figure 1. *A scatter plot of CWM of nitrogen against PC 1. Exclosure plots are in blue and ambient in red. The number above the points refers to the plot number in the study area, Långfjället.*

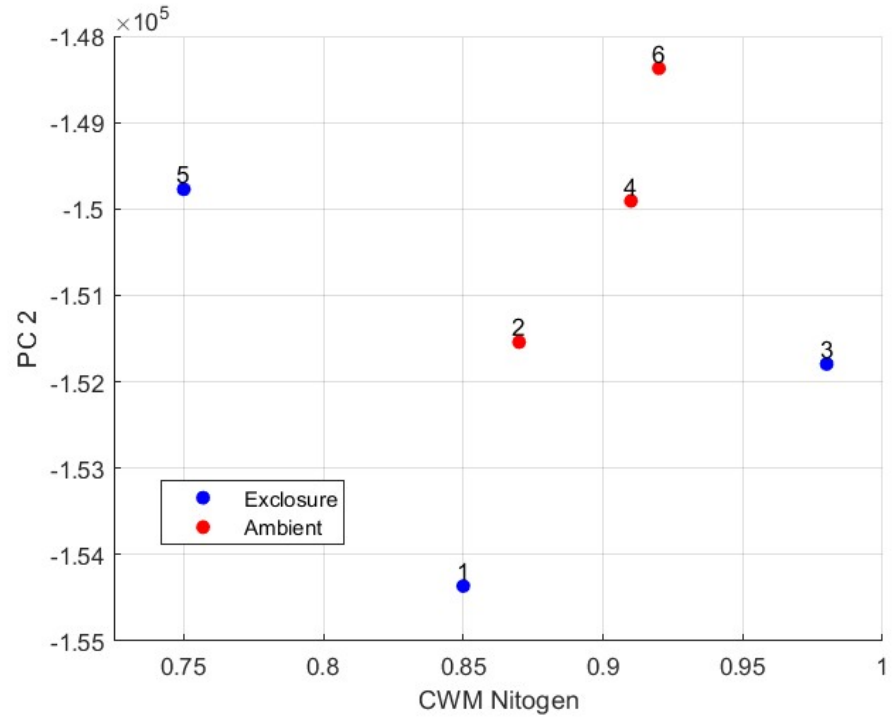

Figure 2. *A scatter plot of CWM of nitrogen against PC 2. Exclosure plots are in blue and ambient in red. The number above the points refers to the plot number in the study area, Långfjället.*

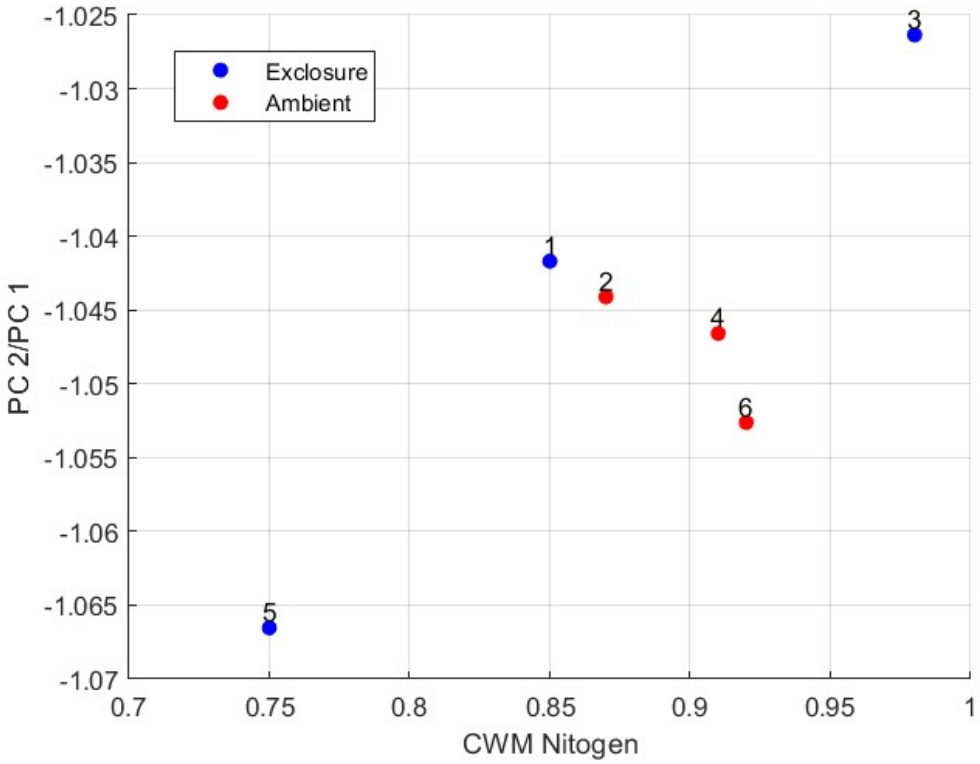

Figure 3. *A scatter plot of CWM of nitrogen against PC2/PC 1. Exclosure plots are in blue and ambient in red. The number above the points refers to the plot number in the study area, Långfjället.*

Appendix 3

Random Forest Regression

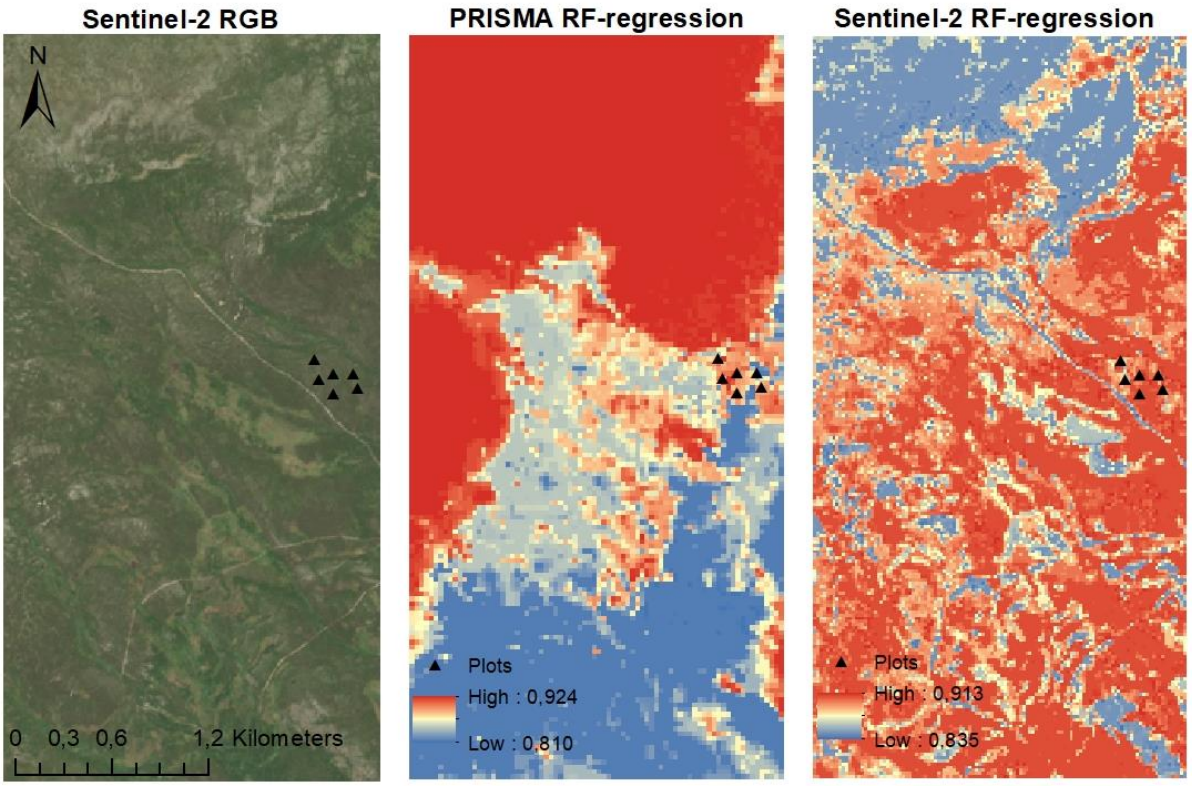

Figure 1. *Maps of RF regression for PRISMA (central figure) and Sentinel-2 (map on the right). PRISMA bands used were: 4, 15, 28, 137, 35, 181, 49 & 165. While Sentinel-2 bands were: B3, B4, B5, B6, B7, B8, B11, B12. The "% var explained" was -45.77 for PRISMA and -41.77 for Sentinel-2. To contextualize the RF classification, result the left map shows a 'True color' background. The black triangles represent the plots in Långfjället.*

Random Forest Classification

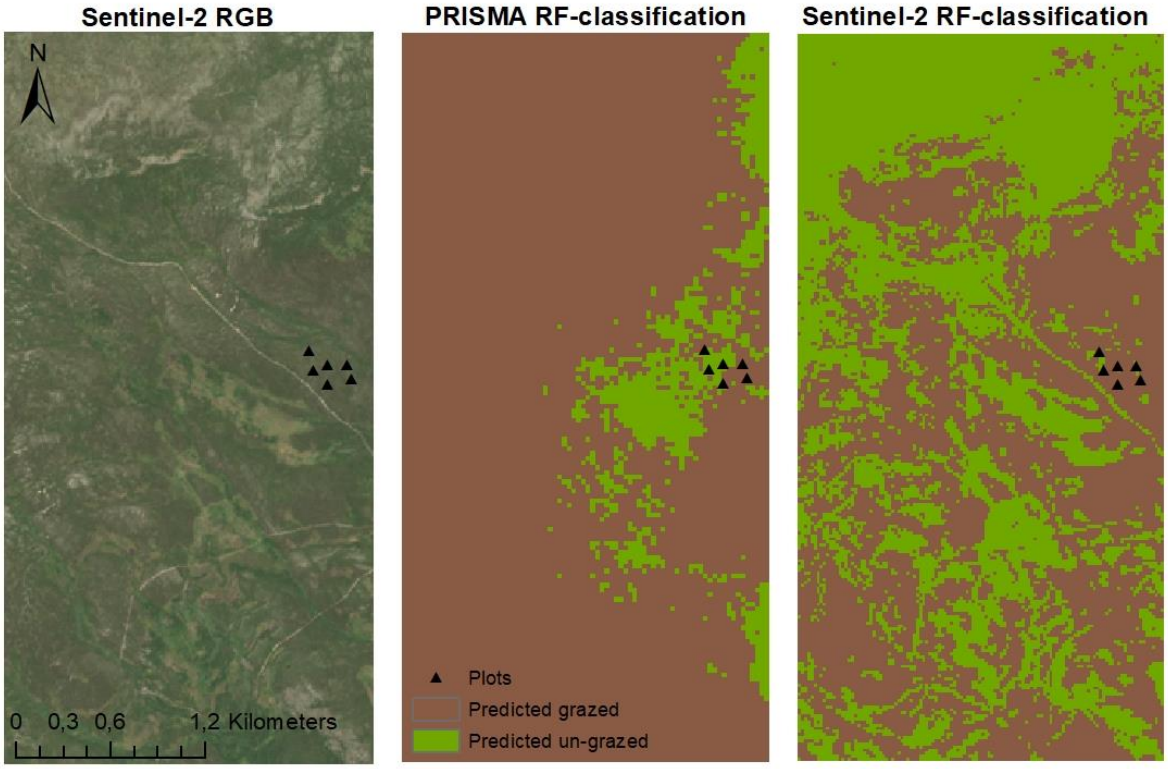

Figure 2. *Maps of RF classification for PRISMA (central figure) and Sentinel-2 (map on the right). PRISMA bands 28 and 49, while Sentinel-2 bands B3, B5, and B7 were used in their respective classifications. With out-of-box errors of 33.33 % for PRISMA and 0 % for Sentinel-2. To contextualize the RF classification, result the left map shows a 'True color' background. Predicted grazed areas are shown in brown and ungrazed areas in green. The black triangles represent the plots in Långfjället.*